Distribution of radioactive elements in the RA-granite bedrock northeast of Säve, Sweden

A comparison with the Änggårdsbergen area of Central Gothenburg

Oscar Samuelsson

Degree of Bachelor of Science
with a major in Earth Sciences
15 hec

Department of Earth Sciences
University of Gothenburg
2023 B-1228

Faculty of Science

UNIVERSITY OF GOTHENBURG

UNIVERSITY OF GOTHENBURG
Department of Earth Sciences
Geovetarcentrum/Earth Science Centre

Distribution of radioactive elements in the RA-granite bedrock northeast of Säve, Sweden

A comparison with the Änggårdsbergen area of Central Gothenburg

Oscar Samuelsson

ISSN 1400-3821

B1228
Bachelor of Science thesis
Göteborg 2023

Mailing address
Geovetarcentrum
S 405 30 Göteborg

Address
Geovetarcentrum
Guldhedsgatan 5A

Telephone
031-786 19 56

Geovetarcentrum
Göteborg University
S-405 30 Göteborg
SWEDEN

Acknowledgements

I would like to extend my gratitude to the people who made this study possible. Thank you to Erik Sturkell for acting as supervisor, and for being available for consultation at odd hours whenever I was in the vicinity. Thank you also to Matthias Konrad-Schmolke for acting as examiner as well as teaching me how to operate the SEM, and to Delia Rösel for helping with thin section treatment and SEM troubleshooting. Thank you Jakob Isaksson for opening doors, giving advice, and operating the larger rock saw.

I would also like to thank my fellow bachelor students Sandra Scekic, Erik Edberg, Carl Teg, Helge Birgerheim and Andreas Ferm for constructive criticism and encouragement.

Finally, I wish to extend my sincere thanks to the people of Stall Norgården for letting me park one evening, despite the late hour and lack of space, to the dogsitters of Rödbo Hunddagis for not letting their dogs run free on my field days after the first incident, and especially to all who came before me for stumbling over obstacles and refining techniques. If I have seen further, it is by standing on the shoulders of giants.

Abstract

This study aims to compare data regarding the spatial distribution of radioactive elements K, U and Th in two exposed areas of the RA-granite, a 1311 ±8 Ma granitic unit unevenly enriched in these elements. Several previous studies have been carried out in the Änggårdsbergen area of Gothenburg, and the results of these were compared with data and physical samples collected from an RA-granite ridge northeast of Säve, roughly 16 km north of Änggårdsbergen but part of the same unit. The spatial relationships observed in the Säve ridge were found to be different from those observed in Änggårdsbergen. Whereas in Änggårdsbergen both U and Th increased to the western part of the area, and no spatial relationship could be detected in the K concentration, in the Säve ridge the K concentration increased markedly in the western part of the area, the U concentration was highest in the middle and east, and the Th concentration was highest in the east. Magnetic susceptibility was also measured and compared, and found to be greatest in the western part of the Säve ridge, in contrast with the central band of increased susceptibility found in Änggårdsbergen. Similarly to studies of Änggårdsbergen, no correlation between magnetic susceptibility and concentration of K, U or Th could be found. However, an increase in U concentration in the rock of the Säve ridge was generally accompanied by an increase in Th concentration.

Analysis of physical samples taken from the Säve ridge showed that U seems to mainly reside in zircon and probably in allanite, whereas Th mainly resides in allanite, monazite and xenotime. Potassium is believed to mainly reside in potassium feldspars, which become less common in areas of lower potassium concentrations. Based on the mineralogy found in analysis of thin sections, the degree of hydrothermal alteration in the rock increases from west to east, with significant breakdown of biotite, iron oxide and titanite to form chlorite and ilmenite.

Sammanfattning

Denna rapport jämför rumslig fördelning av de radioaktiva grundämnena K, U och Th i två olika områden där RA-granit går i dagen. RA-graniten är en 1311 ±8 Ma gammal granitisk enhet som karaktäriseras av förhöjda halter av radioaktiva grundämnen. Flera tidigare studier på RA-graniten har genomförts i Änggårdsbergen, Göteborg, och resultaten från dessa tidigare studier jämfördes med nya data och prover från en RA-granitisk ås nordost om Säve, ca 16 km norr om Änggårdsbergen men i samma stråk. De rumsliga fördelningarna som observerades i Säveåsen visade sig vara annorlunda jämfört med fördelningen i Änggårdsbergen. I Änggårdsbergen ökade U och Th i den västra delen av studieområdet, och ingen tydlig relation kunde observeras i kaliumhalter. I Säveåsen visade sig U vara förhöjt i mitten och östra delen av åsen, Th vara förhöjt i östra delen och K vara tydligt förhöjt i den västra delen av åsen. Vidare uppmättes och jämfördes magnetisk susceptibilitet, och befanns högst i de västra delarna av Säveåsen, till skillnad från det centrala bandet av förhöjd susceptibilitet som uppmätts i Änggårdsbergen. Liksom i tidigare studier i Änggårdsbergen fanns ingen korrelation mellan magnetisk susceptibilitet och K-, U- eller Th-koncentration i Säveåsen. Däremot upptäcktes en generell positiv korrelation mellan uran- och toriumkoncentrationer i Säveåsen.

Analys av bergprov från Säveåsen visar att U främst huseras i zirkon och troligtvis allanit, medan Th huseras i allanit, monazit och xenotim. Kalium finns troligtvis huvudsakligen i kalifältspat, som är mindre vanliga i prover från områden med lägre uppmätta kaliumhalter. Baserat på studier av tunnslip ökar hydrotermal omvandling i Säveåsen mot de östra delarna, och medför betydlig nedbrytning av biotit, järnoxider och titanit och formation av sekundär klorit och ilmenit.

Table of Contents

1. Introduction

1.1 Academic background

A number of previous studies have been carried out on the Gothenburg RA-granite, surveying using handheld gamma spectrometry and magnetic susceptibility instruments (Cooper Svensson & Lundin Frisk, 2018; Elf & Winberg, 2019; Hultin & Håkansson, 2017), but all have been confined to the area of Änggårdsbergen in central Gothenburg.

This has resulted in relatively dense and reliable data over that area, and has uncovered a general increase of U and Th when moving from east to west, illustrated in Figures 1.A and 1.B. Furthermore, an east-westerly variation in magnetic susceptibility has also been found, as shown in Figure 1.C, though the variations in magnetic susceptibility and radioactivity do not appear to be correlated (Elf & Winberg, 2019).

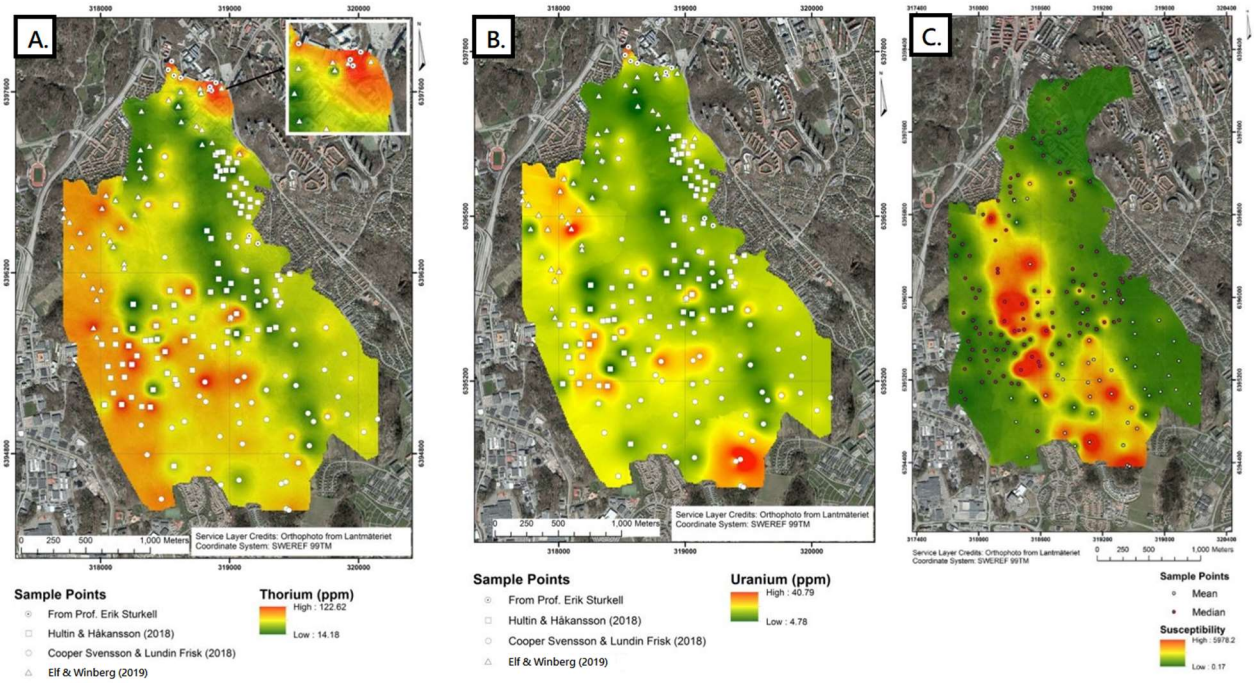

Figure 1: (A) Thorium and (B) Uranium content as well as (C) Magnetic susceptibility in Änggårdsbergen. Modified from Elf and Winberg (2019) using data from several earlier studies.

As Figure 1.C shows, the magnetic susceptibility in Änggårdsbergen has been found to be greater in a band down the middle of the unit. In contrast, the thorium and uranium content of the rocks increases closer to the western edge rather than the middle. Thorium content is generally higher than uranium content, but individual point measurements show U/Th ratios of up to 1,53 (Elf & Winberg, 2019).

In previous studies of the RA-granite, uranium and thorium were found to reside in the accessory minerals zircon, allanite, monazite (Hultin & Håkansson, 2017) and xenotime (Cooper Svensson & Lundin Frisk, 2018).

When all points in the area are plotted on a diagram of percentage of Potassium vs. parts per million of Thorium, a certain bimodality may be observed, illustrated in Figure 2.

When compared with other granitic units in western Sweden, such as Stigfjord granite (blue), Bohus granite (grey) and non-RA granites from central Gothenburg (yellow), the spread of the RA-granite values (orange) is also significant. Whereas a relationship between increase in Potassium and increase in Thorium can be seen in some of the units (GVC, Stigfjord), no such relationship seems to exist in the closely grouped Bohus granites of Bohus-Malmön. Similarly, no Potassium-Thorium relationship has been found in the RA-granites of Änggårdsbergen (Elf & Winberg, 2019).

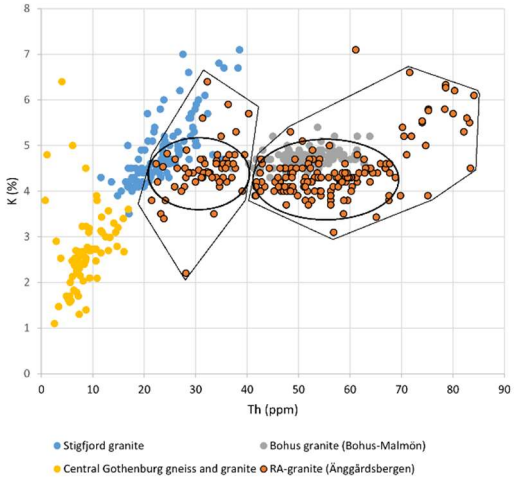

Figure 2: K (%) vs. Th (ppm) for several Swedish granitic units. Bimodal distribution of RA-granite (orange) has been highlighted. Modified from Elf and Winberg (2019).

1.2 Geologic background

1.2.1 Regional Geology

The unit of study is a part of the Sweconorwegian province of western Sweden and southern Norway, which consists of several rock units formed between 1800 Ma and 900 Ma. The study specifically deals with rocks from the Idefjorden terrane, pictured in Figure 3.

The Idefjorden terrane can be subdivided further into several smaller formations and suites, and the area has undergone significant metamorphism in several periods. During the Gothian orogeny of 1650 – 1500 Ma several granites and granitoids intruded, and the area was deformed further during the Sweconorwegian orogeny of 1140 – 900 Ma (Hegardt et al., 2007). In the time between these, several additional intrusions took place. Of these, the most notable for this study is the Kungsbacka bimodal suite, which follows the Göta Älv shear zone (GZ in Figure 3).

The Kungsbacka bimodal suite intruded around 1340 – 1300 Ma, likely in an environment of continental rifting, and includes three granitic units. These are the Askim granite, the Göta granite, and the RA-granite. The former two are closer to the granitic standard in their radioactive element content than the latter (Hegardt et al., 2007), which is the focus of this study.

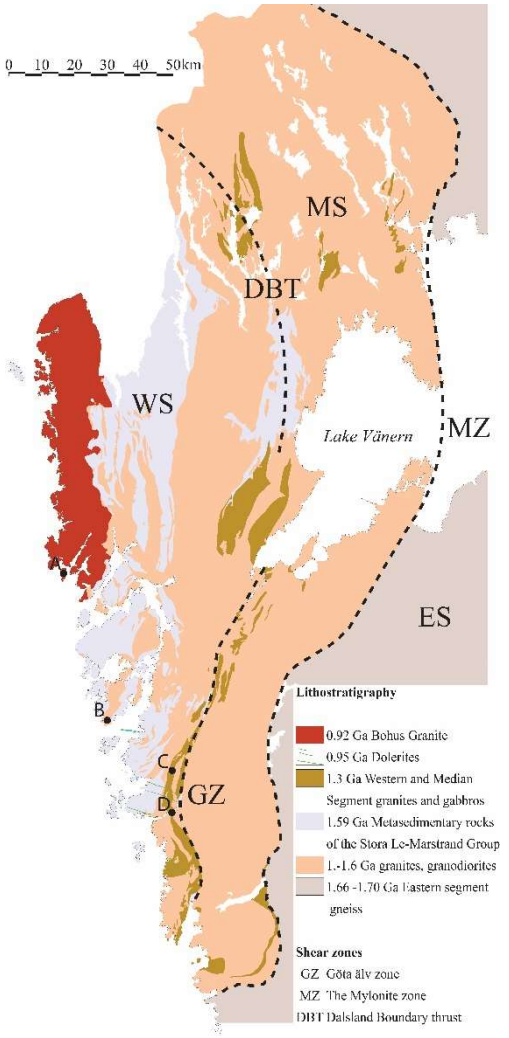

Figure 3: Regional geology of the Idefjorden terrane, western Sweden. The areas of interest to this study are marked as follows: A: Bohus Granite, B: Stigfjord Granite, C: Säve RA-granite, D: Gothenburg. Modified from Sturkell & Hegardt [unpublished], data from SGU.

1.2.2 Unit geology, the RA-granite

The RA-granite, also called in some sources *Gneissose granite from Kungsbacka*, *RA2* or *Kärra granite* and shown in red in Figure 4, is a granitic unit, red to reddish grey in colour and occasionally fluorite-bearing (Samuelsson, 1985). It is mainly characterised by an uneven yet significant enrichment in radioactive elements. This feature has given the unit its name, as RA stands for radioactive. It can be easily distinguished from other rock units by ground or airborne gamma spectrometry, as can be observed in Figure 5, but seems to give way to less radioactive Göta granite further north in the suite.

The northern part of the unit extends north-northeast roughly parallel to the Göta Älv shear zone. Further south, a smaller spur of the RA-granite cuts off from the Göta Älv shear zone, running across the island of Hisingen in parallel with the main unit before ending in south-eastern Hisingen. The main unit continues through central Gothenburg and south to Kungsbacka, with a major outcrop in the Änggårdsbergen nature reserve.

The unit is dated to between 1311±8 and 1325±8 Ma, based on U-Pb dating of zircons (Hegardt et al., 2007). Given its age, it has been deformed by only the Sweconorwegian orogeny, but significantly enough to present a gneissic texture in many places (Samuelsson, 1985).

Studies of the RA-granite of Änggårdsbergen have found it to be peraluminous (Cooper Svensson & Lundin Frisk, 2018; Elf & Winberg, 2019), meaning that the amount of constituent Al_2O_3 is greater than the combined amount of K_2O, Na_2O and CaO (Best, 2003). It has been found to be most similar to anorogenic (A-type) granites (Cooper Svensson & Lundin Frisk, 2018). A-type granites often intrude during continental rifting, which matches the intrusion conditions of the Kungsbacka suite (Hegardt et al., 2007).

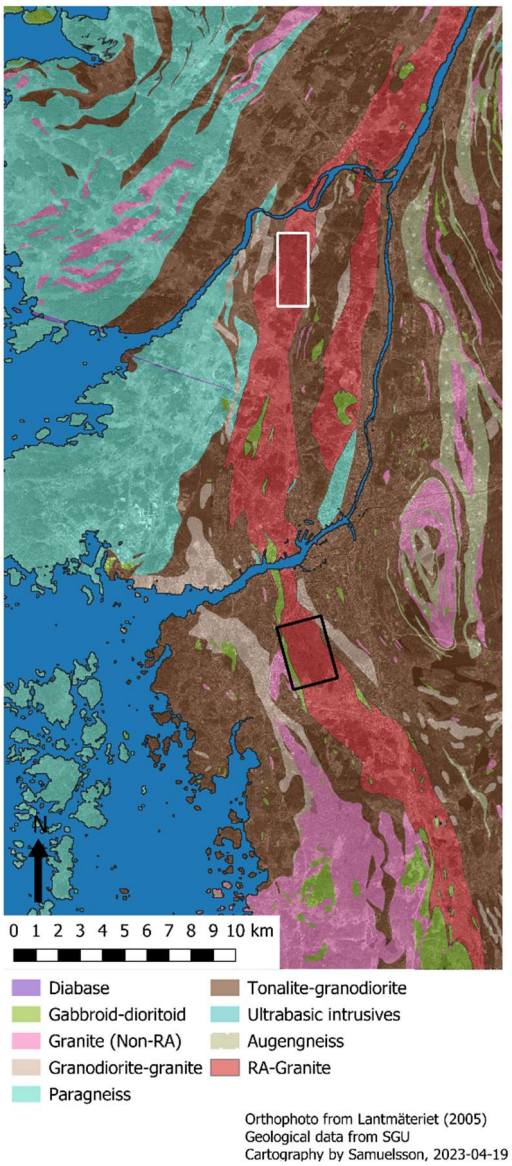

Figure 5: The RA-granite (red) in a simplified geological map of the Gothenburg area. The Änggårdsbergen nature reserve is marked by a black rectangle, and the Säve ridge is marked with a white rectangle.

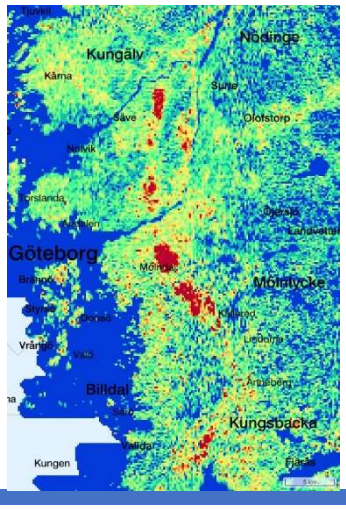

Figure 4: Airborne gamma spectrometry results (Uranium). Data from SGU. Note the high values in central Gothenburg, which is the Änggårdsbergen area.

1.2.3 Metamorphism and alteration

Having undergone deformation and folding during the Sweconorwegian orogeny, the RA-granite is sufficiently deformed to be described as a gneiss in many places. The outer parts of the rock are more or less weathered, commonly to a depth of a centimetre or more, though this effect is somewhat less apparent in places which have been abraded by ice sheets. Occasionally, the rock is weathered in such a way as to become grusified, but this is relatively rare and depends on the amount of secondary clay minerals present in the rock, which must surround other grains to cause grusification (Samuelsson, 1985). Given the extensive abrasion of rock outcrops by ice sheets during the last ice age, grusified gravel is likely to have left the main rock mass after the ice retreated.

Previous studies have found a variety of minerals associated with metamorphism and hydrothermal alteration, such as epidote, titanite and chlorite (Cooper Svensson & Lundin Frisk, 2018; Elf & Winberg, 2019; Samuelsson, 1985). These are often found along fractures, where hydrous solutions are likely to have passed (Elf & Winberg, 2019).

As the rocks in question have been partially metamorphosed, it is prudent to investigate their ratio of uranium to thorium. Under oxidising conditions, uranium forms compounds soluble in water. Thus, hydrothermal alteration under oxidising conditions lowers the U/Th ratio. The same is not true under reducing conditions (Robb, 2021), and in such cases granitic rocks retain the normal U/Th ratio of approximately 0,25 (Rudnick & Fountain, 1994). In previous studies of the RA-granite of Änggårdsbergen, the mean U/Th value of the rock was found to be 0,27 (Cooper Svensson & Lundin Frisk, 2018; Hultin & Håkansson, 2017), which is close enough to 0,25 as to be considered normal.

1.3 Study area

With earlier studies mainly being limited to the exposed RA-granite of Änggårdsbergen, the question of whether the relationships observed there could extend to different parts of the unit became relevant. Further north in the unit, on the island of Hisingen, several large rocky outcrops were present. From these, a north-south ridge located northeast of the town of Säve was chosen for examination.

To best test the potential for east-west variations like those seen in Änggårdsbergen, a 0,9 km east-west transect was chosen across the northern part of the ridge. The site was chosen primarily for plentiful rock exposure, but also for the relatively sparse ground vegetation, which made traversal easier. Coincidentally, a natural fracture valley ran immediately to the south of the transect, roughly parallel to it. This valley provided a fine landmark for navigation as well as a footpath for easier travel to and from sites.

A satellite image of the ridge with the transect marked can be seen in Figure 6.

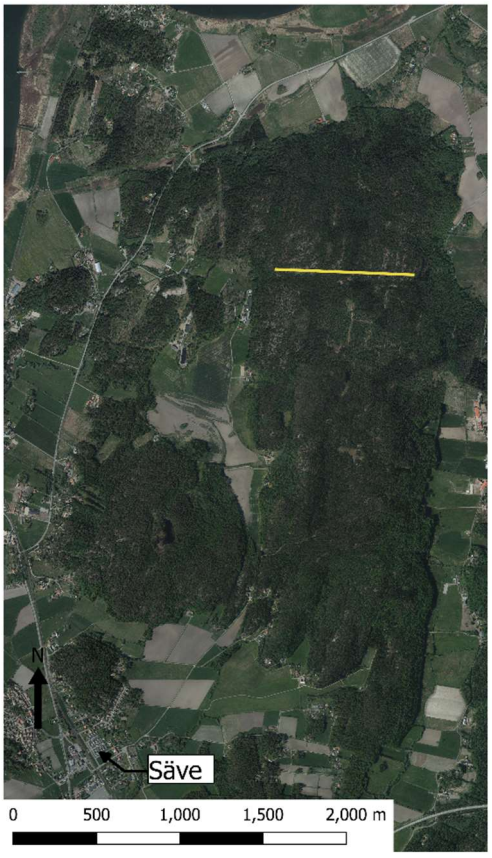

Figure 6: The Säve ridge, with the transect marked as a 0,9 km yellow line. Orthophoto from Lantmäteriet.

1.4 Gamma spectrometry

Gamma spectrometry is a method whereby gamma rays emitted by radioactive elements can be used to determine the concentration of those elements in a medium. Briefly explained, it functions by allowing gamma photons to enter a detector, where the number of counts within certain intervals of energy are recorded. The resulting spectrum is used to calculate concentrations of radioactive elements in the sample (Wallbrink et al., 2003).

In field use, gamma spectrometry can be carried by hand, as in this study, or mounted on aircraft in order to cover larger areas. Since all radiation is decreased in magnitude by distance, airborne gamma spectrometry can aid in surveying large areas to search for radioactive element enrichment (Finck, 1992) but is not sufficiently exact to accurately determine the exact content of radioactive elements in the underlying rock, nor to show variations on anything but the regional scale or greater.

Handheld gamma spectrometry results in comparatively precise point measurements (Kock & Samuelsson, 2011) but is also more prone to influence by very local anomalies, the so-called nugget effect. To avoid this, several measurements are usually carried out at every site, with some spatial separation, and a mean value taken. Additionally, for the results to be of highest quality and precision the surface measured must be dry, as water can shield the instrument from gamma radiation. Lastly, the surface must be flat or very nearly so, as the instrument gathers radiation from a wide radius and the resulting reading will be increased or decreased as more or less radioactive medium is present within that radius.

1.5 Magnetic susceptibility

Magnetic susceptibility is the ability of a material to accept magnetization in a magnetic field. It is a dimensionless quantity, as the ratio of induced magnetization to inducing magnetic field (Tauxe et al., 2018). The magnetic susceptibility of rock mass is dependent on the magnetic susceptibility of the constituent minerals. Ferromagnetic minerals such as pentlandite, pyrrhotite and especially magnetite raise the magnetic susceptibility, whereas their absence lowers it (Rosenblum & Brownfield, 1999).

Of these, the only mineral confirmed to be present in previous studies of the RA-granite is magnetite (Elf & Winberg, 2019; Hultin & Håkansson, 2017).

2. Method

2.1 Field work

2.1.1 Point measurements

Point measurements were taken in the field, with at least three readings of the gamma spectrometer per site and between 9 and 16 readings of the magnetic susceptibility, with greater variation in measured values necessitating more readings in order to produce an accurate mean value. Since gamma spectrometry functions best on dry and flat rock surfaces with little to no surrounding topography, care was taken in choosing the measurement sites in order to get the highest data quality possible. As the area provided plentiful rock exposure, with many smooth surfaces, the resulting measurement sites are all considered to be of excellent quality.

A dense line of 63 sample points was taken close to the east-westerly fracture. A second, thinner line of 10 points was made significantly further north in order to test whether any variations ran along the lines of foliation or extended in any other directions, as any and all variations would seem east-westerly if point measurements were only taken along a single line.

To prevent the possibility of the nugget effect distorting the data, at least three gamma spectrometry readings were carried out at each point in the shape of a triangle. Each of the three gamma spectrometry assays per point were allowed to run for 180 seconds in order to minimise potential errors in measurement. This time span has been judged as appropriate for the concentrations of radioactive elements present in the RA-granite, and was used by Elf and Winberg (2019) and Hultin and Håkansson (2017).

Figure 7: RS-230 BGO Super-Spec (left) and SM-20 (right), pictured in the field.

The gamma spectrometer used was the Radiation Solutions Inc. model RS-230 BGO Super-SPEC, and the magnetic susceptibilimeter used was the Gf Instruments SM-20. Both instruments are pictured in Figure 7.

A Garmin Oregon 300 handheld GPS was used to record the coordinates of each point measurement. Points were named by the format XX YY ZZZ, where XX records the year of measurement, YY the measuring researcher and ZZZ the point number. Thus, the first point collected would be named 23OS001.

2.1.2 Physical sampling

Three samples were taken from the rock of the ridge, one on the western side, one in the middle and one in the east. These correspond to point measurements 23OS001, 23OS003 and 23OS004, and are shown in Figure 8. Care was taken to procure enough unweathered rock material, as the weathered edges reached several centimetres below the rock surface on occasion.

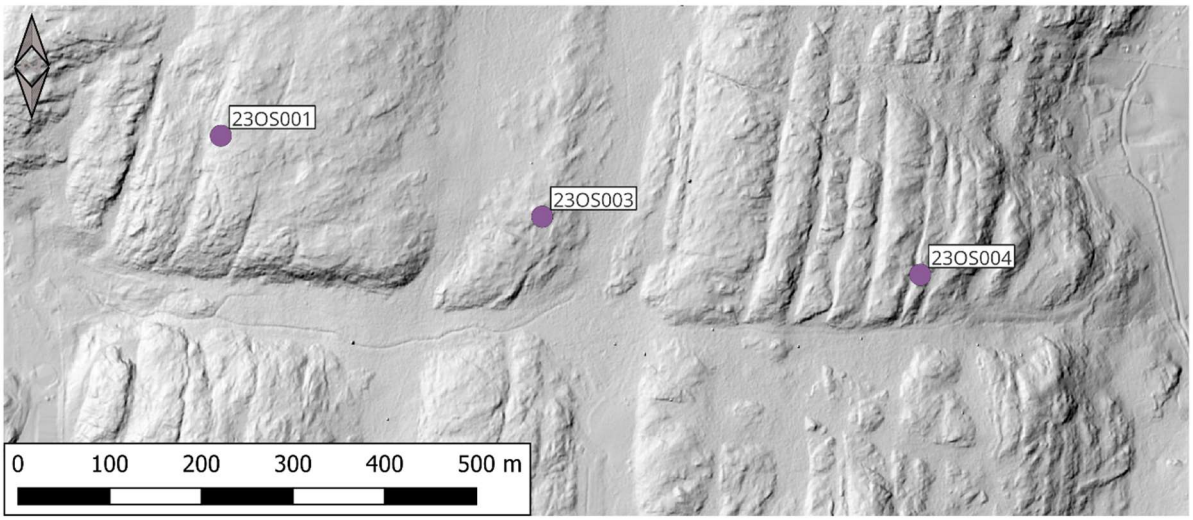

Figure 8: Location of the physical sample sites on the Säve ridge.

2.2 Thin section microscopy and chemical analysis

Slices roughly 1,5-2 centimetres thick were sawed in the lab from the samples taken in the field, and the weathered edges discarded. Of the remainder, rough rectangular shapes were made to measure the dimensions of a standard thin section, save thickness. These were sawed so that the cut would display the greatest possible variety of structures and minerals. The rough sections were packaged and sent to Thin Section Laboratory in Toul, France, where they were prepared into polished thin sections and returned.

From the remaining rock, samples were sent to ALS Chemlab laboratory in Piteå, where they were logged before being crushed to the point that 70% or more passed through a 2 mm sieve, split using a riffle splitter and each split pulverised to the point that 85% or more passed through a 75 µm sieve. Following this, the samples were subjected to the Complete Characterisation Package of tests, CCP-PKG01, designed to combine a great number of tests in order to establish the sample concentrations of major elements, carbon and sulphur, trace elements, volatile trace elements, and base metals.

Chemical data produced by these analyses were sent back, normalised by CI chondrite values of McDonough and Sun (1995), and used to compare the REE concentrations of each rock sample. As this had been done by the same laboratory for many other RA-granite samples from Änggårdsbergen, the values could be easily compared. Similarly, sample concentrations of major elements were also compared with those of Änggårdsbergen.

Thin sections were examined by polarised light microscope, as well as by Scanning Electron Microscope (SEM).

2.3 Data processing and GIS

From the multiple measurements of magnetic susceptibility and gamma spectrometry on each site, a mean value was computed and assigned to the points using Microsoft Excel. Since the SM-20 susceptibilimeter records magnetic susceptibility as 10^{-3} SI units, the resulting mean values were multiplied by 10^3 to get the true susceptibility.

These mean values and coordinates were compiled and used to create a shapefile in QGIS for interpolation and visualisation. For the interpolation, the inverse distance weighing (IDW) tool was used, and the standard distance coefficient of 2.

Using mean values of potassium and thorium content, the points gathered from the Säve RA-granite were plotted together with the Änggårdsbergen RA-granite and three other granitic units in a K (%) vs. Th (ppm) diagram, and the results were compared between units. Additionally, the point values from the Säve ridge were further subdivided by area in U/Th, K/U and K/Th diagrams, allowing for comparison of potential groupings.

Finally, topographic charts were created using point means from Änggårdsbergen and Säve, and used as background images in K/Th diagrams to aid in visualising the number of points present despite extensive overlap. These were created by calculating the number of points present in a 0,5% K * 5 ppm Th pixel in a K (%) vs Th (ppm) diagram, and resulted in isolines for five, ten and fifteen points per pixel.

3. Results

3.1 Gamma spectrometry

3.1.1 Potassium (K)

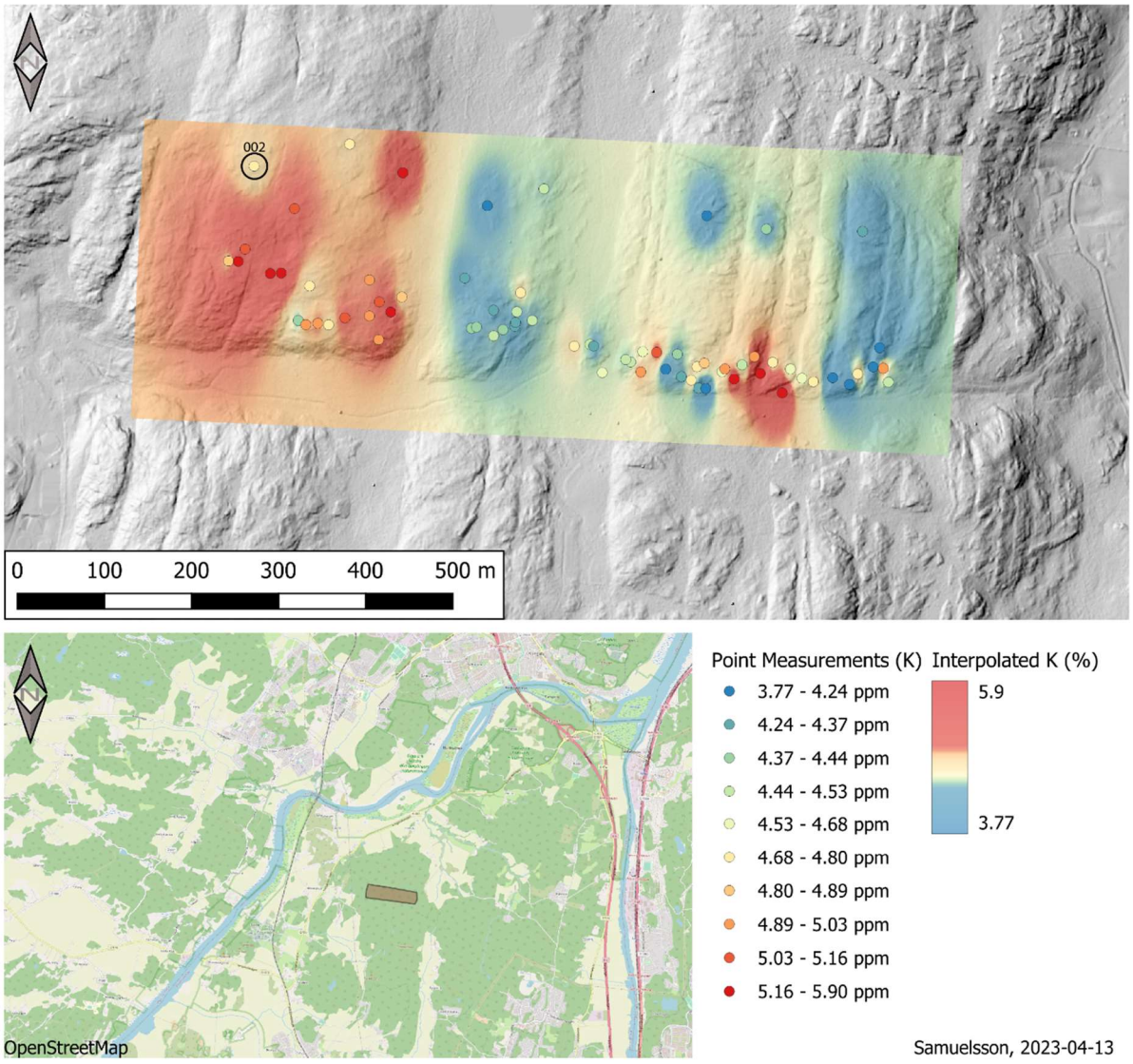

Figure 9: Point measurements and interpolated rock potassium content, measured as percentage. Note the generally higher K in the western part of the map, as well as the smaller red area in the eastern part of the map. Point 002, furthest to the northwest, has been marked and represents a slightly smaller value (4,73%) than expected for the area.

Potassium concentrations of the point measurements range from 3,77 to 5,90% K, with one major area of high values and one minor, as illustrated in Figure 9. In the western part of the map, medium to high values are the norm, and a smaller section in the eastern part of the map also produces high values.

Based on the interpolated values, there does seem to be some sort of variation in the east-west direction. However, as shown in the middle and eastern part of the upper row of points in Figure 9, the variation does not appear to be exclusively in the east-west direction but may also have some north-south component.

The individual measurements used to calculate these mean values can be found in Appendix II.

3.1.2 Uranium (U)

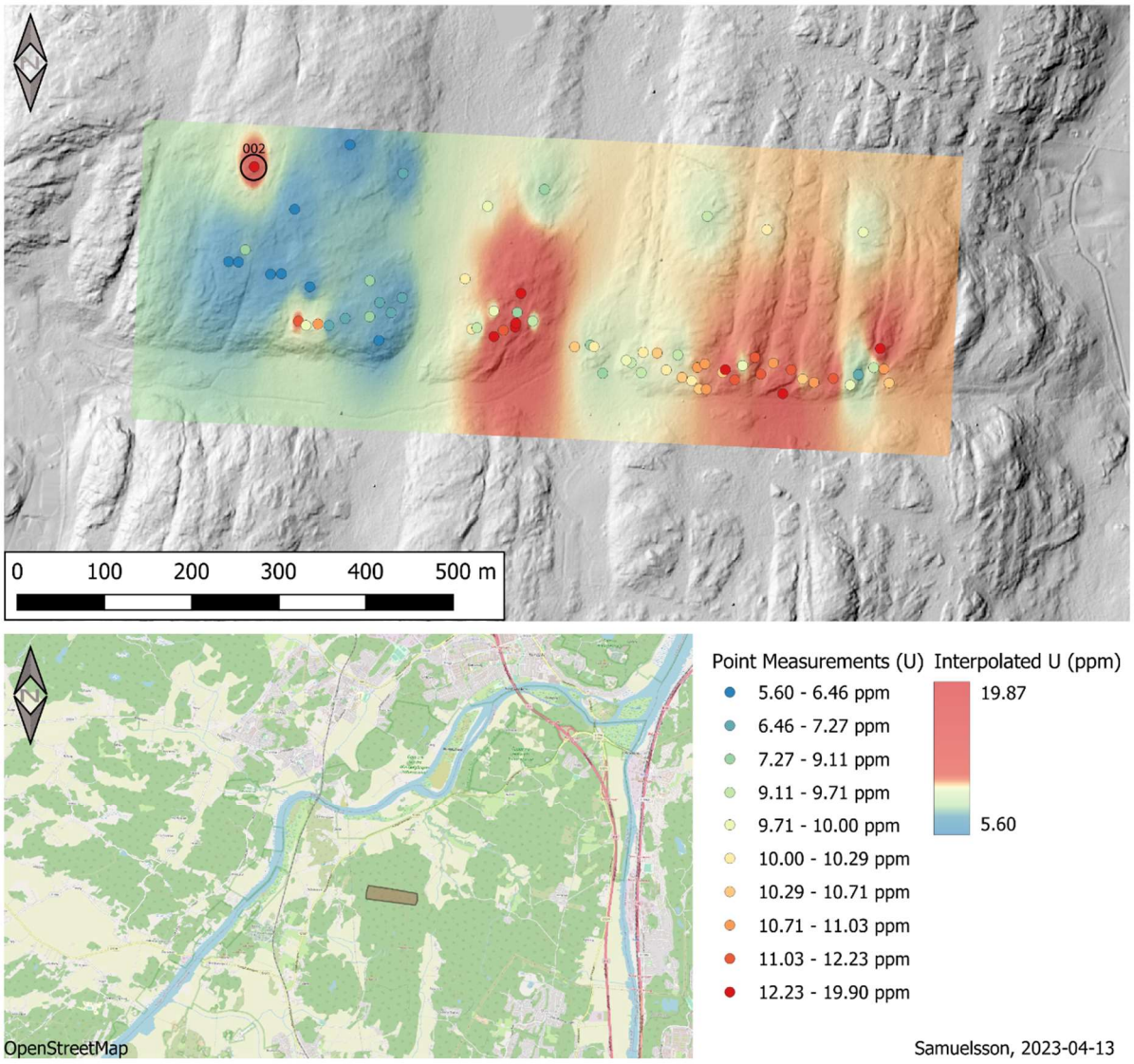

Figure 10: Point measurements and interpolated rock uranium content, measured as ppm. Note the generally higher U in the eastern part of the map, as well as the band of high concentrations in the centre. Point 002, furthest to the northwest, has been marked and represents an unexpectedly high value in an otherwise low-value area.

As illustrated in Figure 10, there appears to be an east-westerly variation in the uranium content of the rock of the Säve ridge. However, rather than increasing to the west or southwest, as in Änggårdsbergen, the trend appears to be the opposite, with a decrease in uranium towards the west and two bands of high concentrations in the centre and east.

Point 002, located furthest to the northwest in the western part of the map, represents a high uranium concentration (12,63 ppm) in an area of otherwise low values. Save for this point, concentrations of uranium in general seem higher to the south, though this may be an artefact of the denser sampling further south.

The individual measurements used to calculate these mean values can be found in Appendix II.

3.1.3 Thorium (Th)

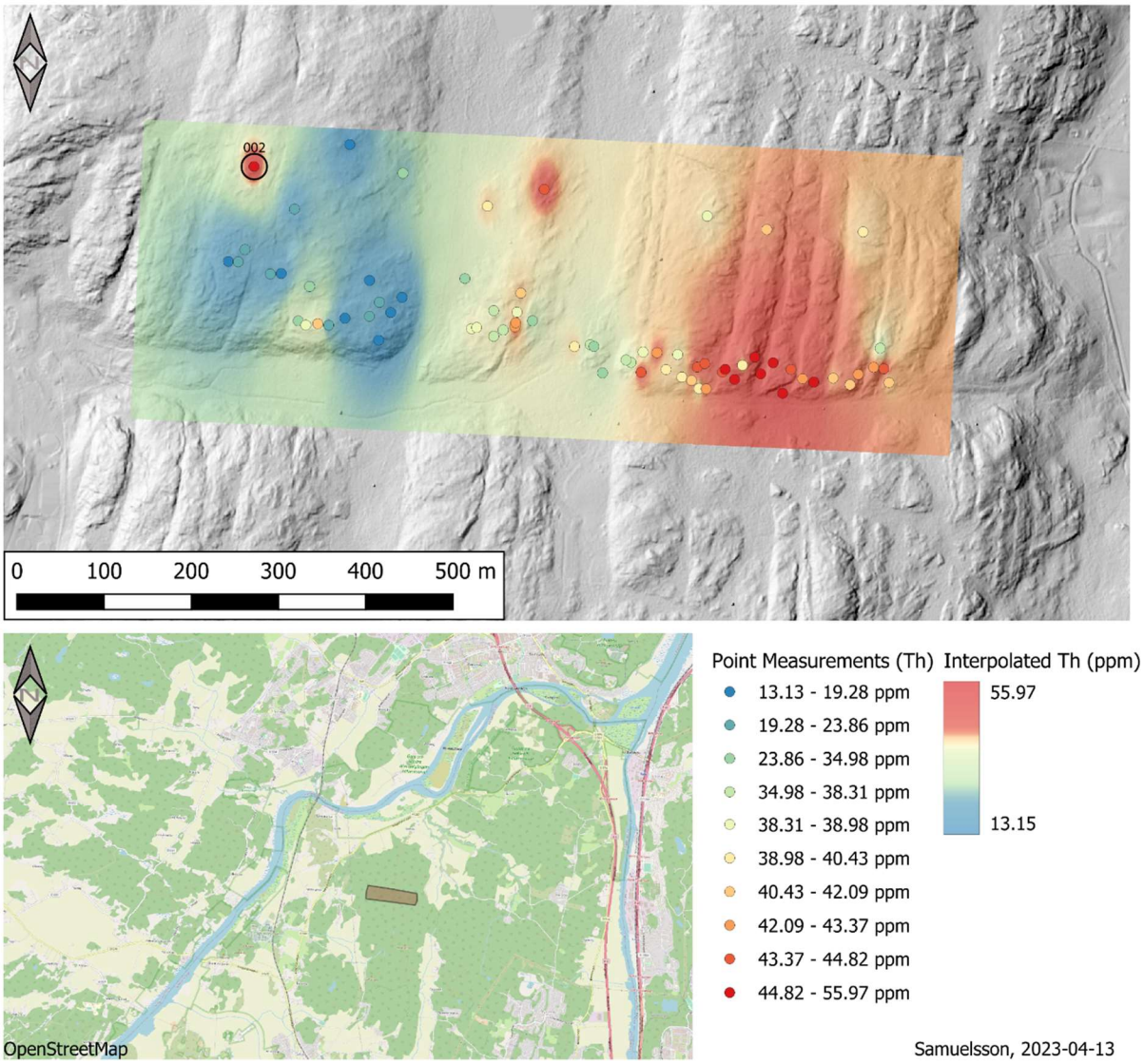

Figure 11: Point measurements and interpolated rock thorium content, measured as ppm. Note the generally higher Th in the eastern part of the map. Point 002, furthest to the northwest, has been marked and represents an unexpectedly high value in an otherwise low-value area.

As illustrated in Figure 11, there appears to be an east-westerly variation in the thorium content of the rock, and similarly to the uranium, the trend appears to be opposite that of Änggårdsbergen. Thorium content appears to decrease towards the west, with the highest values present in the eastern part of the study area, save for one outlier.

The outlier mentioned is point 002, which shows a similarly unexpectedly high thorium concentration (47,3 ppm) as uranium concentration, see section 3.1.2.

The individual measurements used to calculate these mean values can be found in Appendix II.

3.1.4 Potassium / Thorium characteristics

Using gamma spectrometry data points from Elf and Winberg (2019), Hultin and Håkansson (2017), Cooper Svensson and Lundin Frisk (2018), Tennby (2016) and Johansson (2014), plotted by the constituent potassium (K) and thorium (Th), rough groupings of granitic rocks can be detected. Figure 12 shows a total of 572 points, divided into five groups by their location and rock type.

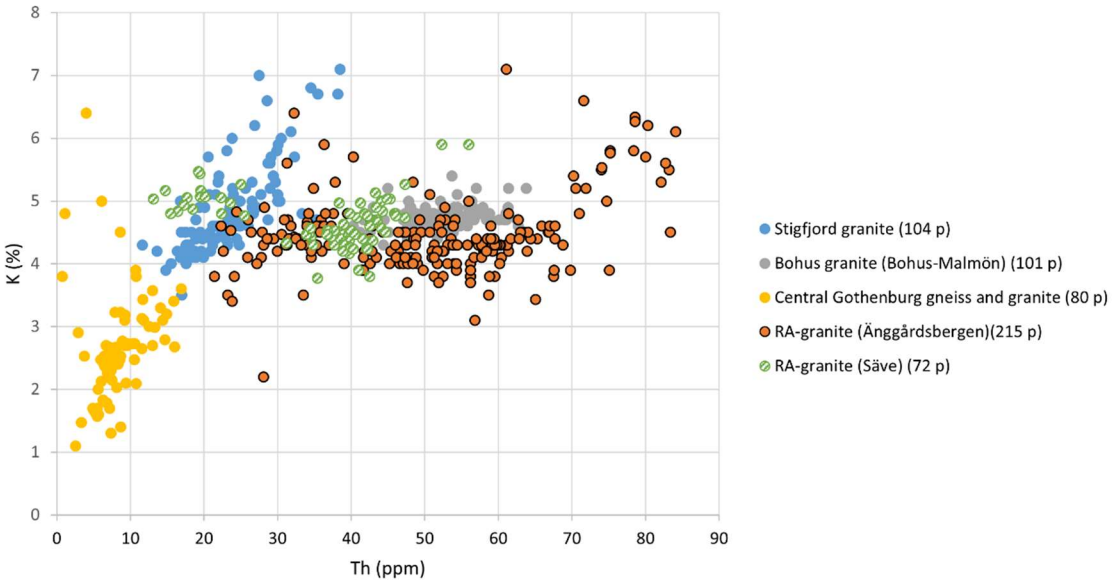

Figure 12: Potassium – Thorium diagram of several granitic units, including the Säve RA-granite. Note the somewhat bimodal distribution and generally lower thorium content when compared to the Änggårdsbergen RA-granite. All data points represent mean values of at least three measurements.

As shown in Figure 12, both the rocks of central Gothenburg and the Stigfjord granites show some relationship between potassium and thorium content, with an increase in one usually corresponding to an increase in the other, barring a few outliers. This is seemingly not the case with the RA-granite of Änggårdsbergen, nor with the Bohus granite of Bohus-Malmön.

Notably, the values of the Änggårdsbergen RA-granite appears to form two groupings of roughly equal potassium content, but above or below 40 ppm thorium. This is possible to discern with just the points, as in Figure 2, but is more easily observed in a topographical chart, such as Figure 13. Additionally, a topographical chart allows for a better sense of the number of points overlapping in a given area.

When compared to these previously collected values, the RA-granite of Säve examined in this study appears to bridge the gap somewhat with respect to the two groupings of RA-granite in Änggårdsbergen. Generally, the values of potassium are similar to the Änggårdsbergen Ra-granite and the Bohus granite of Bohus-Malmön, whereas the values of thorium are generally slightly lower, lacking the extremes of the RA-granite found in Änggårdsbergen.

Similarly to the previous values, no relationship between potassium and thorium content could be detected in Säve.

Notably, the Säve RA-granite appears to display a similarly bimodal distribution when compared to the Änggårdsbergen RA-granite. This is not as easy to see, due to the smaller sample size (72 points in Säve, 215 in Änggårdsbergen). For ease of viewing, all raw points and their means have been

plotted in Figure 13, resulting in a more comparable 290 points. As illustrated in Figure 13, this makes the bimodal distribution a great deal more obvious.

Also of note, both groups of RA-granite show roughly the same potassium value, and the bimodal distribution of the Säve points appears much like that of the Änggårdsbergen points, save for a reduction of around 10 ppm thorium.

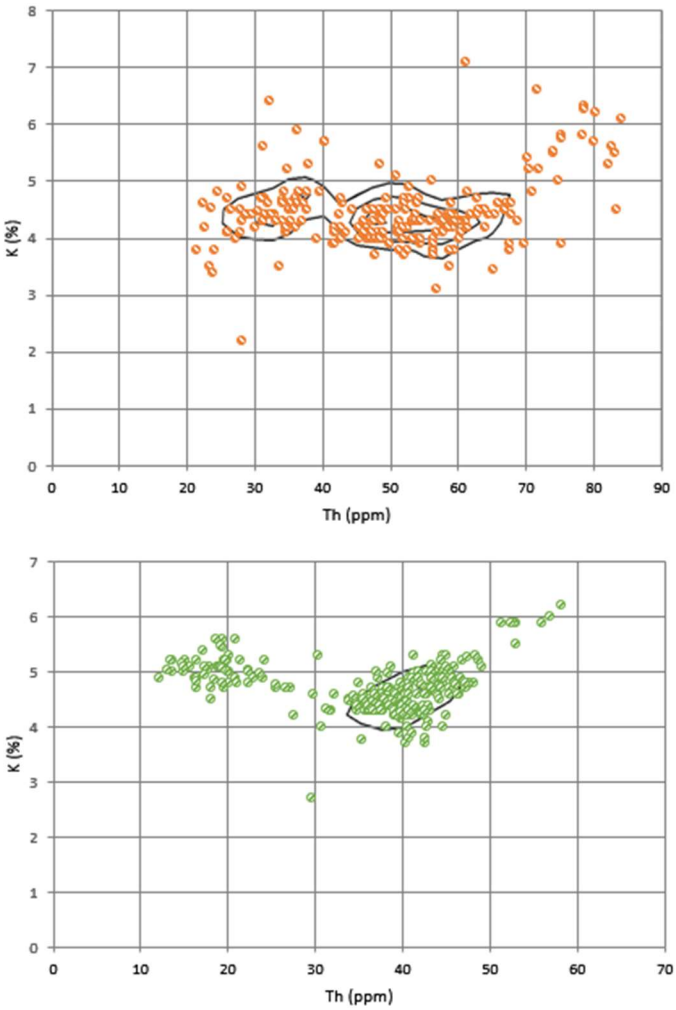

*Figure 13: Topographic K-Th charts of Änggårdsbergen (above) and Säve (below). Contour lines of five mean points per 0,5%*5ppm pixel. Note that the lower chart contains mean points and their constituent values, resulting in 290 values, in order to make the bimodal distribution more visible.*

3.2 Magnetic susceptibility

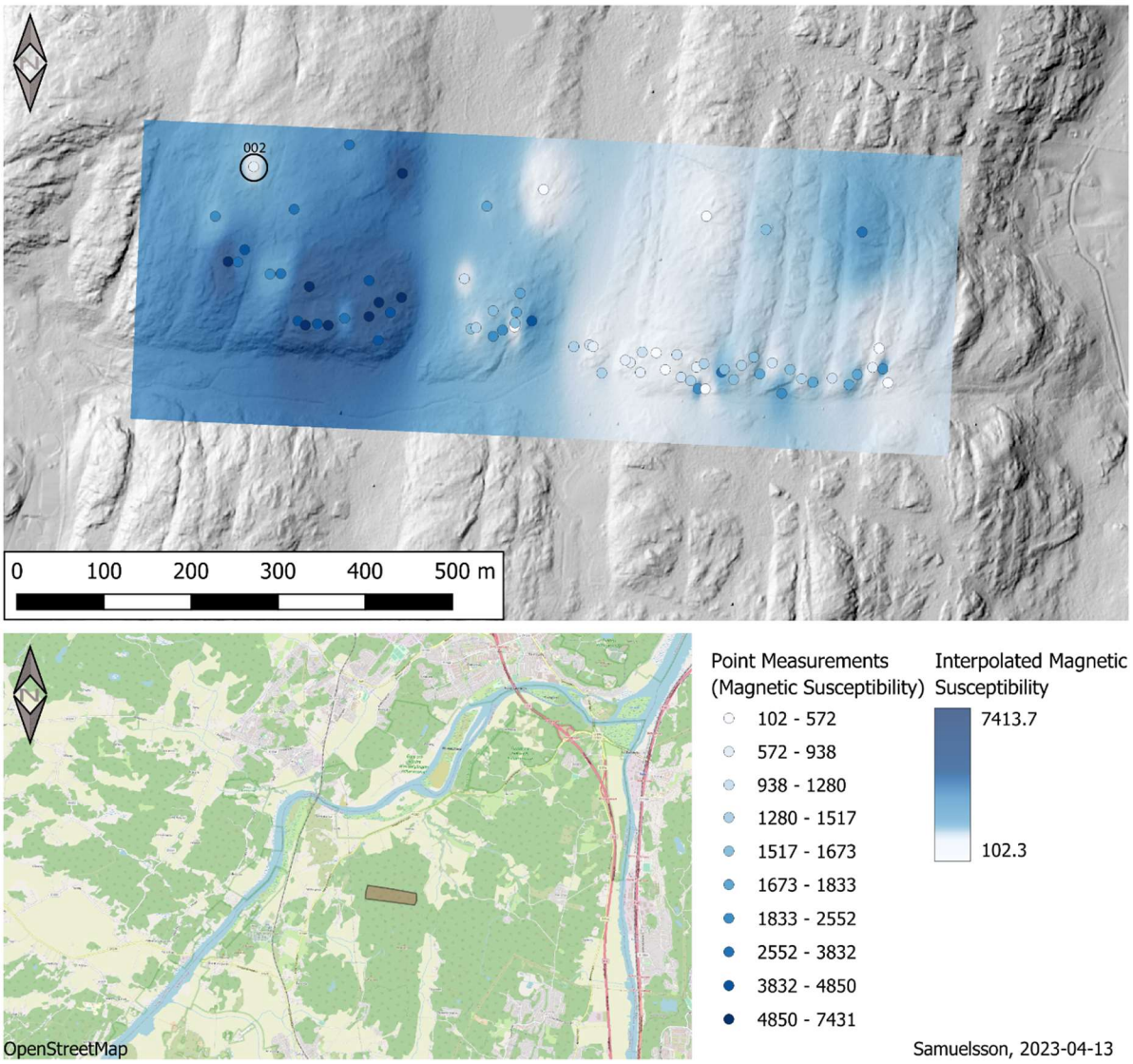

Figure 14: Point measurements and interpolated magnetic susceptibility. Note the generally lower values to the east. Point 002, furthest to the northwest, has been marked and represents an unexpectedly low value in an otherwise high-value area.

The magnetic susceptibility of the Säve ridge rock is generally low in the east and high in the west, as illustrated in Figure 14.

Point 002, furthest to the north and west, is a point of low magnetic susceptibility. Aside from point 002, the western sub-ridge is surprisingly uniform in high values of magnetic susceptibility.

The individual measurements used to calculate these mean values can be found in Appendix II.

3.3 Relationship analysis

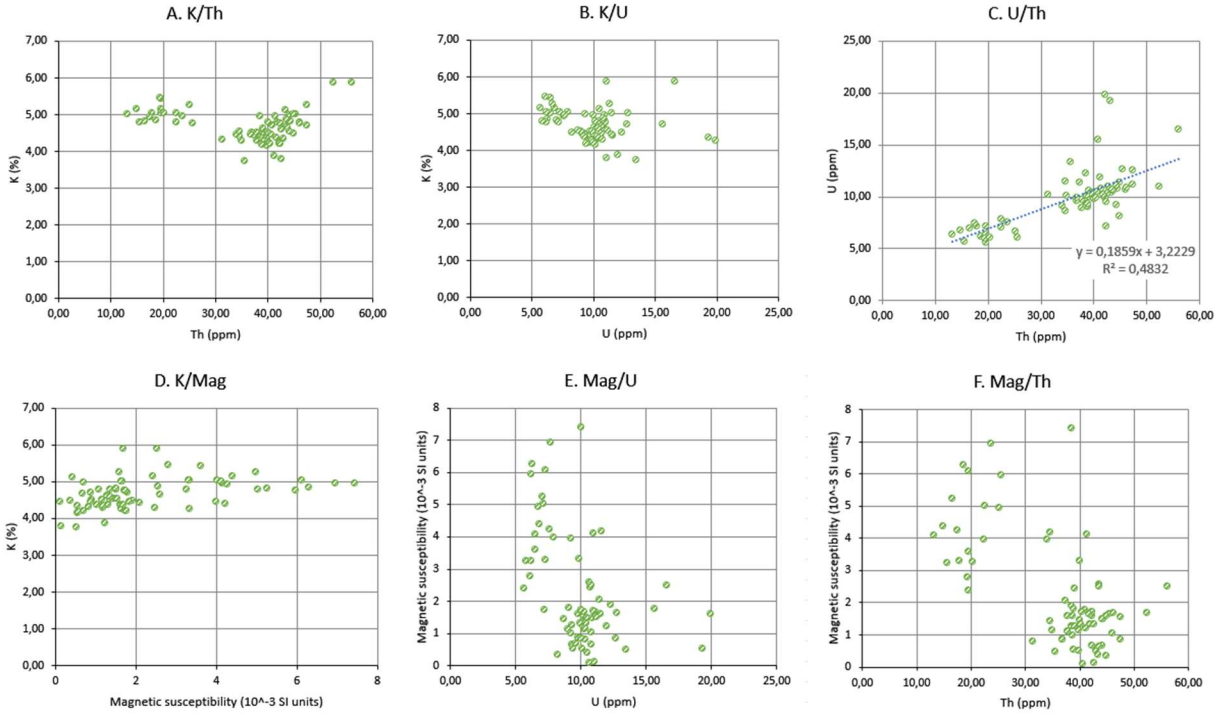

Figure 15: Relationship diagrams between the Potassium, Uranium and Thorium content and the Magnetic Susceptibility of the Säve RA-granite. No clear relationship between magnetic susceptibility and any other variable can be seen.

Figure 15 shows six relationship diagrams for the four variables of potassium content, thorium content, uranium content and magnetic susceptibility.

As can be seen in Figures 15.D – F, there seems to be no relationship between the magnetic susceptibility and any other variable. However, bimodality (previously mentioned in section 3.1.4) is apparent in all three relationship diagrams of radioactive elements (Figure 15.A – C), albeit much clearer in 15.A and 15.C than in 15.B.

As for the relationship between concentrations of radioactive elements, the uranium-thorium diagram is the only one to show an apparent relationship between change in one variable and a corresponding change in another. Increased concentrations of uranium generally accompany increased concentrations of thorium as seen in Figure 15.C. A trendline was constructed to fit the perceived relationship, with the following formula:

$$\mathrm{U\ (ppm)} = 0{,}1859 * \mathrm{Th\ (ppm)} + 3{,}2229$$

When the same process is applied to data from Änggårdsbergen, as in Figure 16, the resulting trend formula is:

$$\mathrm{U\ (ppm)} = 0{,}1996 * \mathrm{Th\ (ppm)} + 2{,}6841$$

which is very similar to the U/Th relationship formula in Säve.

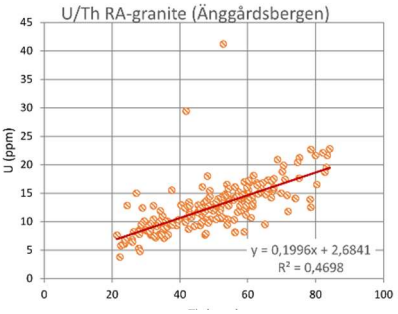

Figure 16: Uranium-Thorium relationship diagram of the Änggårdsbergen RA-granite. Note the similar formula to Figure 15.C.

3.4 Radioactive element ratios over the study area

The U/Th ratio of the study points ranges from 0,170 to 0,490 with a mean value of 0,287, compared to the mean value of 0,27 in Änggårdsbergen. Of the 72 points with relevant data, 46 show U/Th values greater than 0,25 with the remaining 26 showing values lesser than 0,25.

When plotted using their corresponding coordinates, as in Figure 17, it is possible to see certain spatial relationships. For example, the western part of the map has just one U/Th value of less than 0,25, whereas the number of greater and lesser values is more equal in the east.

Discounting those upper points taken on the western sub-ridge, all upper points show lower U/Th than 0.25. This may be an artefact of less dense sampling, or possibly an indication of further alteration or leaching near the main fracture, where it is likely that more water has flowed.

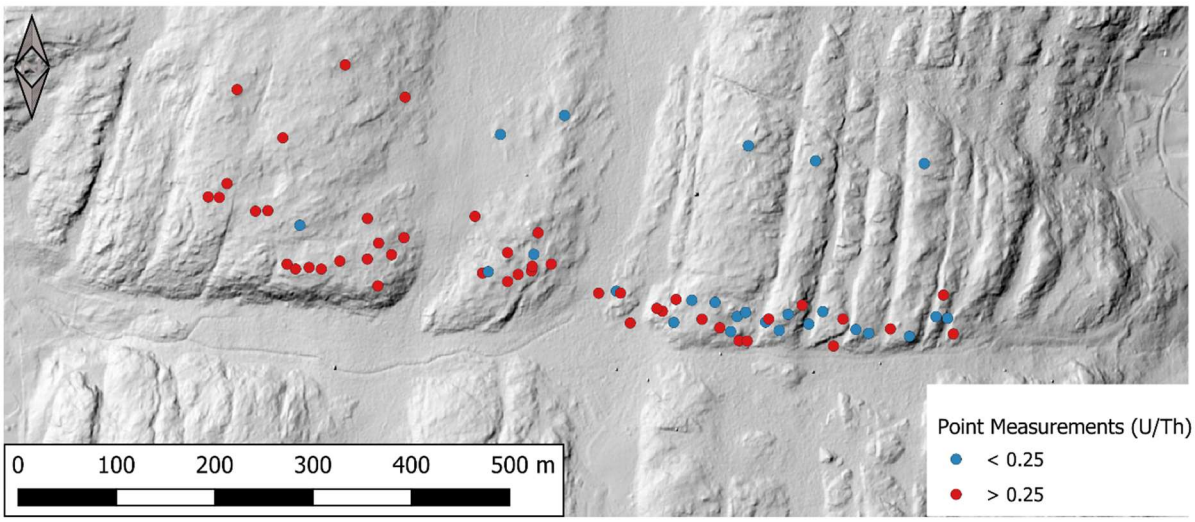

Figure 17: U/Th ratios over the study area. Note how the western section has just one point with a value below 0,25, whereas the middle and eastern section are more varied.

In fact, the western part of the ridge stands out in more than the U/Th ratio. As illustrated in Figure 18, the point measurements of the western part of the ridge (in blue, with black rims) form the smaller, separate grouping previously seen in Figure 15.A-C. By contrast, points collected from the central and western parts of the ridge form overlapping groupings in all radioactive element ratio diagrams.

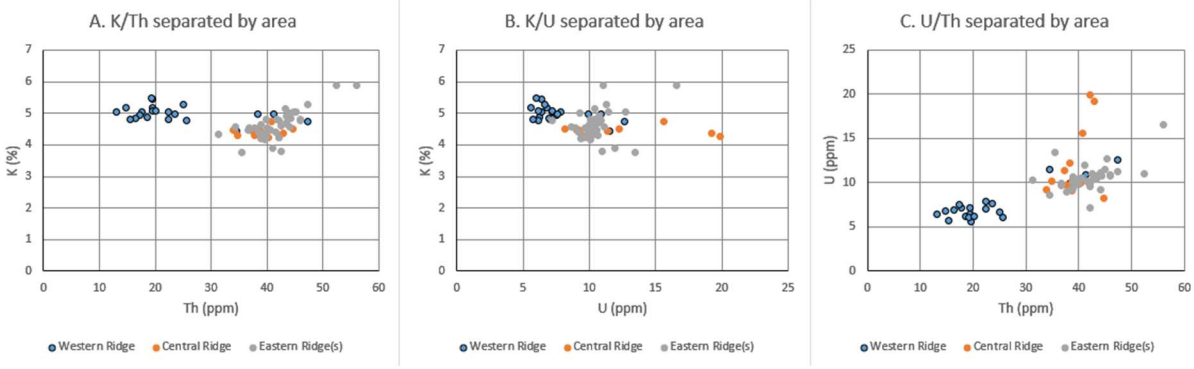

Figure 18: Area separated radioactive element ratio diagrams. Note the western ridge points (blue, black rims) forming a distinct smaller grouping, contrasted by the greatly overlapping central and eastern ridge points.

3.5 Chemical analysis

Chemical analysis of samples 23OS001, 23OS003 and 23OS004 yielded interesting results. As shown in Figure 19, samples 23OS003 and 23OS004 were essentially identical in REE concentrations. In contrast, sample 23OS001, taken in the westernmost part of the ridge, shows significantly lower concentrations of all REEs.

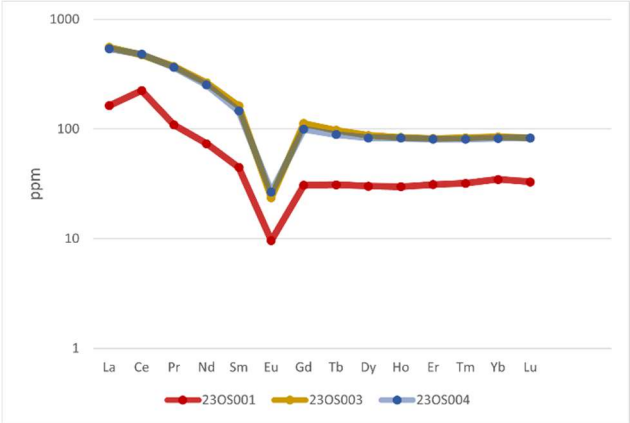

Figure 19: Chondrite normalized REE values of the three Säve Samples, logarithmic. Note the extreme overlap in samples 23OS003 and 23OS004.

When combined with a selection of the many samples taken from Änggårdsbergen during previous studies, as in Figure 20, it is clear that the REE values of the Säve ridge samples do not stand out when compared to rocks sampled in Änggårdsbergen. The low europium, for example, is present in all samples and of roughly equal proportion when compared with the other concentrations of the samples.

All three samples show a peraluminous composition, similarly to samples from Änggårdsbergen, with values of 1,34, 1,27 and 1,37 respectively. Such values are similar to those found in Änggårdsbergen, as illustrated in Figure 21.

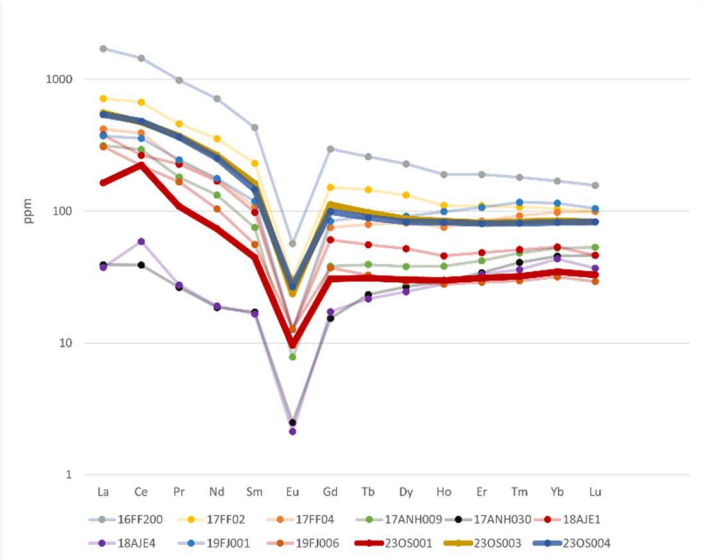

Figure 20: Chondrite normalised REE values of three Säve samples and a further nine Änggårdsbergen samples.

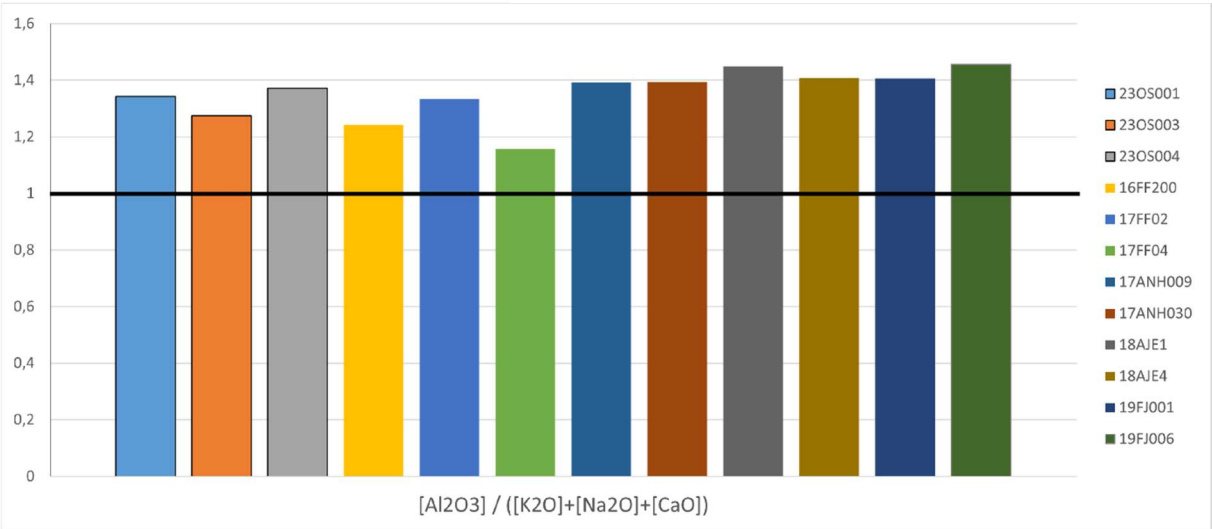

Figure 21: Comparison of samples from Säve and Änggårdsbergen, showing the ratio of alumina to potassium, calcium and sodium. Note the uniformly high values, showing peraluminous compositions.

When comparing concentrations of major elements in the samples from the Säve ridge, as in Figure 22, it should be noted that sample 23OS001 (yellow, black squares) seems to present higher concentrations of calcium and magnesium when compared to 23OS003 and 23OS004.

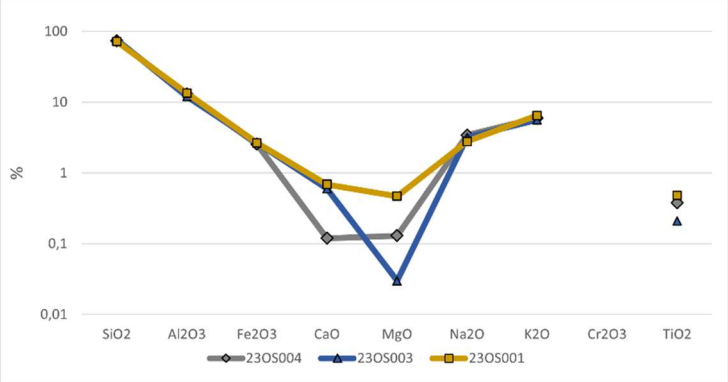

Figure 22: Major element oxide concentrations in samples from the Säve ridge.

Though the significantly lower magnesium concentration in sample 23OS003 (0,03% MgO, as compared to 0,47% MgO in 23OS001), and lack of detectable chromium concentrations in all Säve samples might seem to be of importance, they do not stand out greatly when compared to samples from Änggårdsbergen, as illustrated in Figure 23. Interestingly, save for detectable or nondetectable chromium levels the main difference between RA-granite samples is essentially just the calcium and magnesium concentrations. Calcium concentration ranges from 5,68% to 0,06%, and magnesium concentration ranges from 2,22% to 0,02%. All other major elements are comparatively similar in concentration between samples. All chemical data can be found in Appendix II.

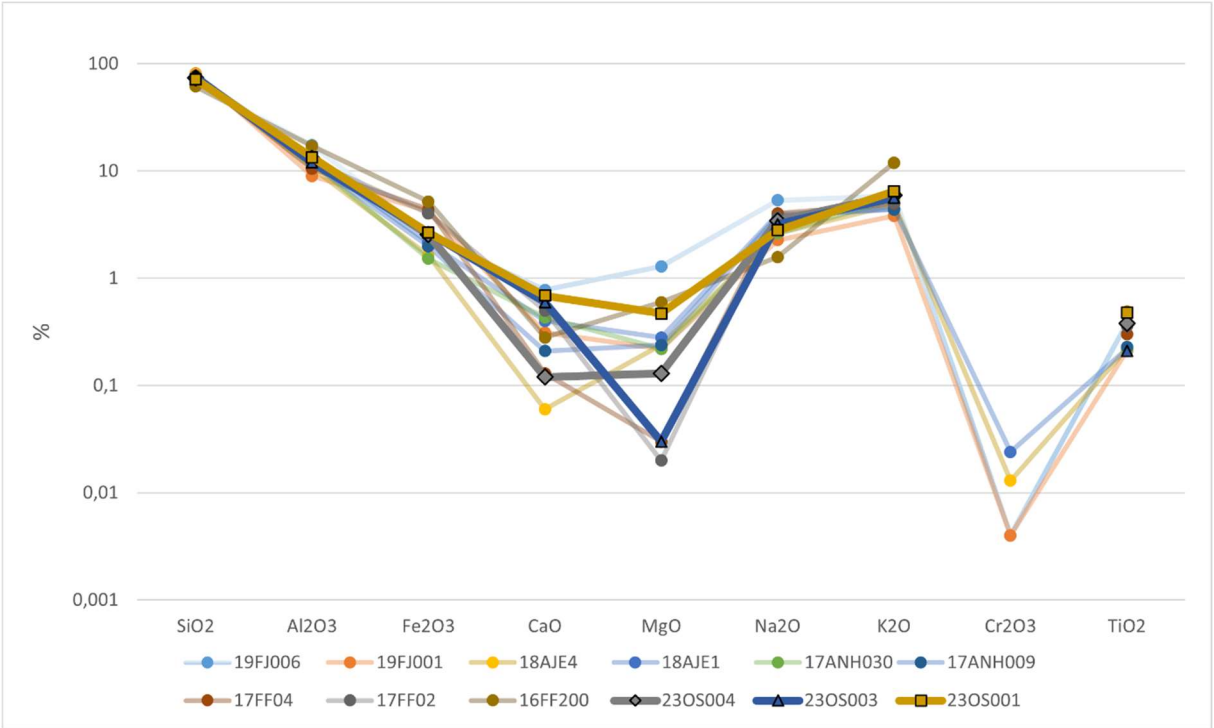

Figure 23: Major element oxide concentrations, Säve ridge and Änggårdsbergen.

3.6 Structural analysis of thin sections

Sample 23OS001, the westernmost of the physical samples, is slightly more finely grained than 23OS003 and 23OS004. 23OS001 additionally shows occasional larger grains, likely corresponding to the small augen of around 1 cm which can be seen in fresh fracture surfaces of the rock in the field.

All samples show some mineral orientation, primarily visible in the orientation of biotite but present in essentially all elongated grains. This orientation is more obvious in samples 23OS001 than in 23OS003 and 23OS004, but is nonetheless present even in these.

Sample 23OS004, pictured in Figure 24, is noticeably more fractured than the other two, with one major and at least one minor fracture parallel to the mineral orientation. In this sample, and only this sample, a significant amount of the grains are missing from the thin section around the corners, likely having been removed during abrasion due to comparatively lower grain-to-grain cohesion. A full image of sample 23OS004 can be found in Appendix I.

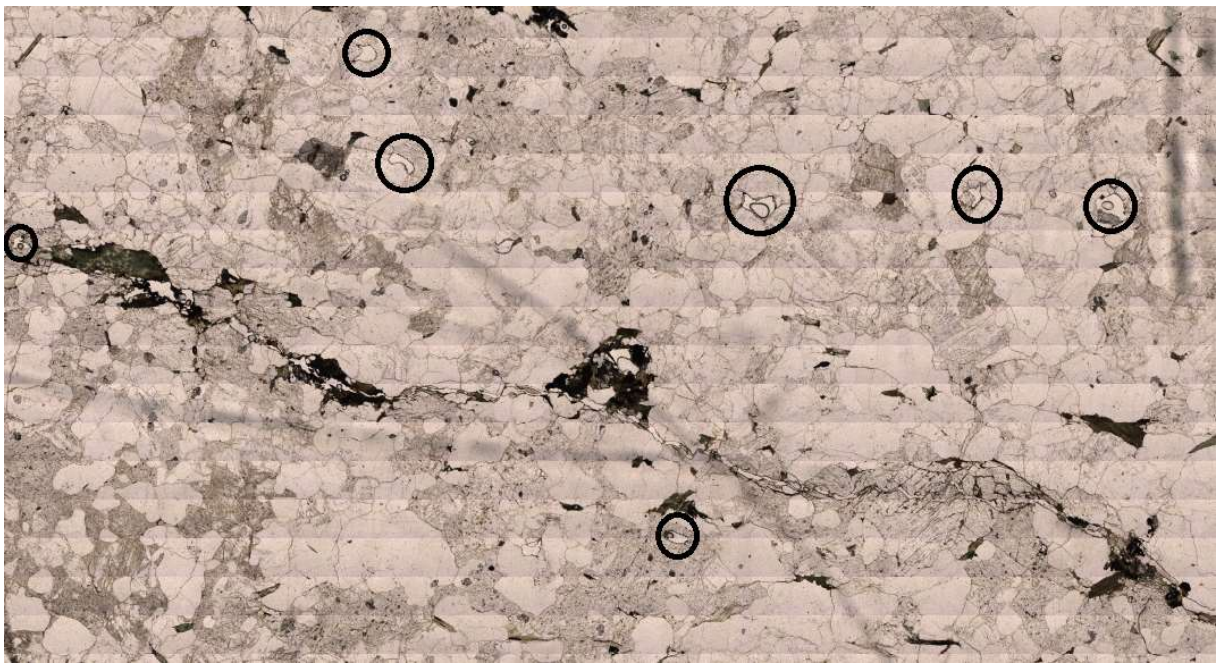

Figure 24: Detail of 23OS004 under plane polarised light. Missing grains are marked by black circles. Note the clustering of dark minerals around the fracture running from central left to lower right. Full image of sample can be found in Appendix I.

3.7 Mineralogical analysis of thin sections

3.7.1 23OS001

Sample 23OS001 is predominantly composed of quartz, potassium feldspars and plagioclase, with some biotite. Plagioclase grains were found to house mainly Na, with smaller amounts of Ca, leading to a classification of albite or oligoclase. Quartz grains in the sample are generally at least somewhat rounded, sometimes of irregular shape, and often show undulose extinction. Potassium feldspar and plagioclase grains are often more elongated than quartz grains and commonly display twinning, but not always.

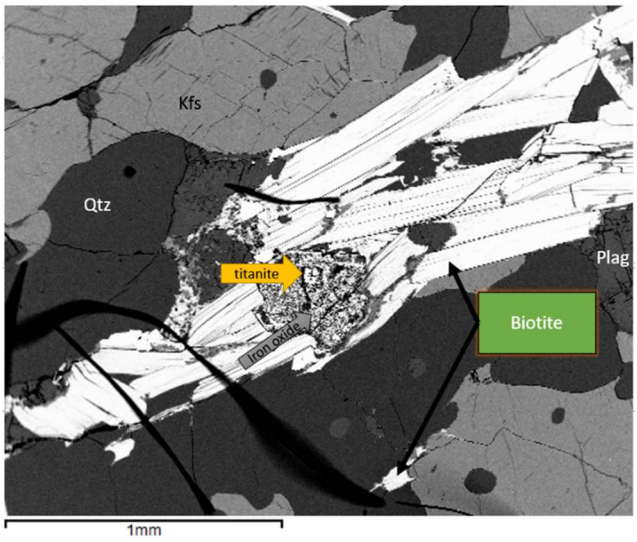

Figure 25: Titanite in iron oxide, surrounded by biotite. Note the small titanite grains in the messy FeO grain.

Biotite in the sample appears in streaks, running roughly diagonally along the thin section, and commonly contains low amounts of Ti. Messy, bloblike grains of iron oxides speckled with small titanite grains are commonly found immediately around biotite grains. An example of these structures can be found in Figure 25.

More well-formed grains of iron oxides, likely hematite or magnetite, as well as titanite, are rare but present in the sample. Like the less well-formed grains of their kind, these too are usually associated with biotite.

Minor accessory minerals zircon and fluorapatite are rarely found in the sample. Fluorapatites were found only in three sites, all small grains immediately adjacent to biotite and FeO-titanite grains.

Zircons found in the sample and examined under SEM were occasionally found to contain Hf and Th, which was the only source of Th found in the sample. Whilst the zircons were found to usually be associated with the FeO-titanite grains, small zircons were also found as inclusions in potassium feldspar and plagioclase grains.

3.7.2 23OS003

Sample 23OS003 is similar to 23OS001 in most aspects, but does present some slight differences.

Though it is mainly composed of quartz and potassium feldspar, the amount of potassium feldspar is lower compared to 23OS001. Plagioclase is present but significantly rarer. Biotite is present in roughly equal amount in 23OS001 and 23OS003, and displays a similar texture.

Four larger grains (0,5-1,5 mm) of well-formed iron oxide are found in the sample. These are likely hematite since the sample showed a lower magnetic susceptibility than 23OS001, and contain smaller inclusions of ilmenite, as seen in Figure 26. Besides ilmenite, Ti is present in the form of titanite, both in the manner of 23OS001 and as larger, more well-developed grains.

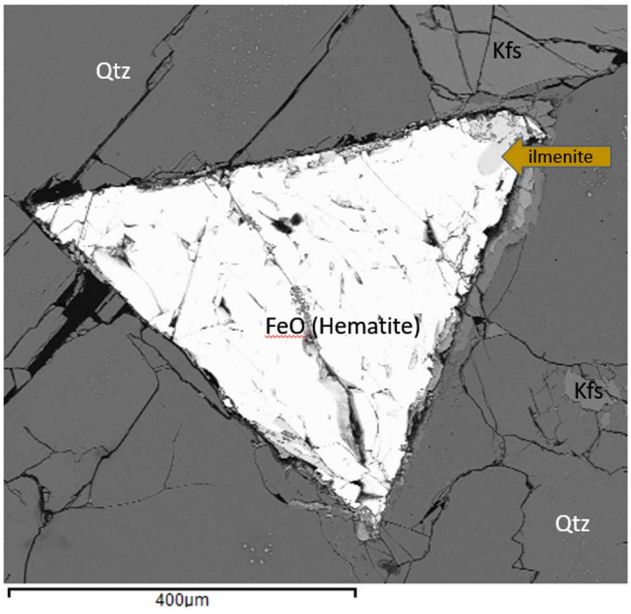

Figure 26: Well formed grain of iron oxide (likely hematite) with ilmenite around some edges and as inclusions.

Fluorapatite is present in roughly the same amount as in 23OS001, which is to say very rare. As in the previous sample, it is found to be associated with FeO-titanite.

As might be expected from the increased radioactivity (see section 3.1), sample 23OS003 contains significantly more zircon than 23OS001. These zircon grains are commonly larger as well, as illustrated in Figure 27, but can still be found as small grains, although much more numerous.

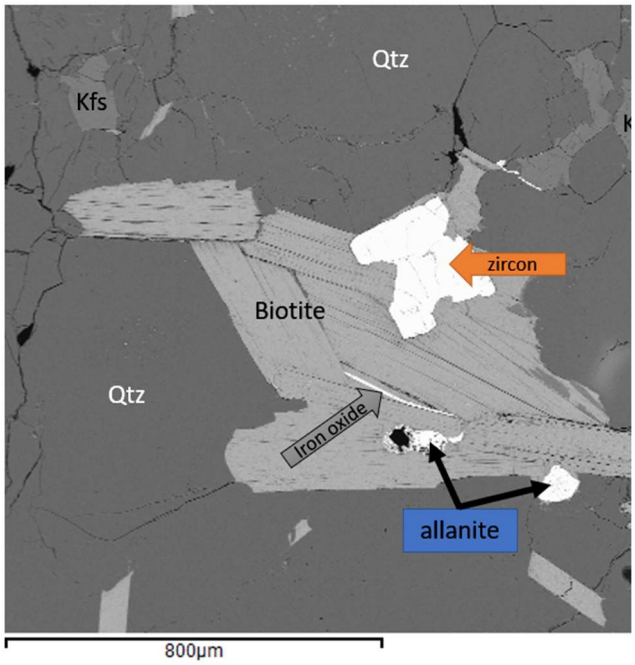

Figure 27: Zircon, allanite and iron oxide grains in biotite.

Allanite was found to be rare but present in the sample, usually as small grains in or around the edges of other grains as illustrated in Figure 24. It is most commonly found with biotite and FeO-titanite grains.

Interestingly, despite the very similar REE content, as seen in Figure 19, sample 23OS003 resembles 23OS001 more than 23OS004 in every way save the increased amount of zircon and iron oxides, and the presence of ilmenite and allanite.

3.7.3 23OS004

Sample 23OS004 is significantly more altered than the other two samples, especially along fractures, and contains certain minerals which are not present in 23OS001 and 23OS003. For example, the RA-granite is known to occasionally be fluorite-bearing, and small fluorite grains can be found in sample 23OS004, albeit very rarely.

Chlorite is common in the sample as clinochlore-chamosite, fully or nearly fully replacing the biotite seen in other samples, especially along fractures.

Grains of ilmenite were also found along fractures, with the growth pattern and shapes indicating the grains to be secondary. As no iron oxides can be found in sample 23OS004, it is assumed that the grains of iron oxide and FeO-titanite present in sample 23OS001 and 23OS003 have broken down in sample 23OS004 and their components used in forming ilmenite.

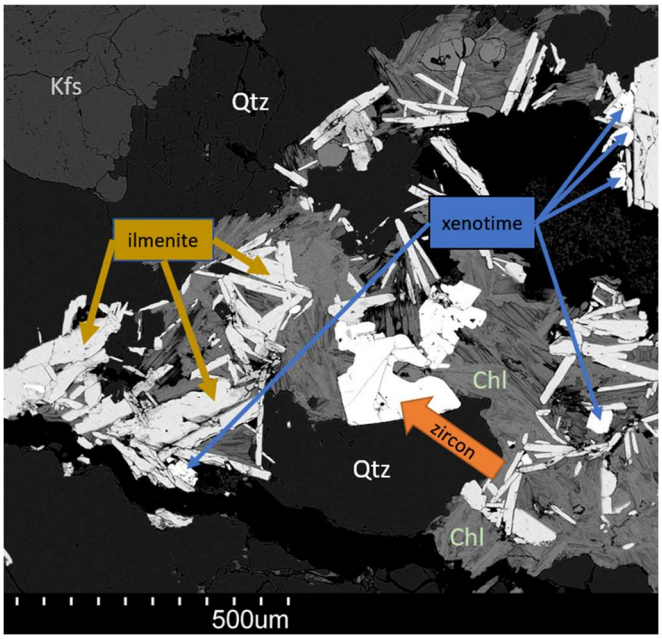

Figure 28: Mineral complex of chlorite, ilmenite, zircon and xenotime along fracture. This same complex can be found in the central portion of figure 21.

Similarly to sample 23OS003, grains of zircon are present in 23OS004, frequently found associated with chloritized biotite and other accessory minerals. When analysed in SEM, these zircons commonly show high concentrations of radioactive elements. Zircons from sample 23OS004 are notable for being the only grains from any of the three samples to, on occasion, show a measurable U content under SEM.

In contrast to sample 23OS003, no allanite was found in this thin section. REE are instead housed in xenotime and monazite, which were not plentiful but neither uncommon. They were often found with ilmenite, chloritized biotite and sometimes each other, though not always as can be observed in Figure 28. In the cases where they were found together, monazite grains tended to be larger than xenotime grains, though xenotime grains were more common.

Rather than potassium feldspar being the dominant feldspar, the most common feldspar grains are ‘dirty’ albite grains containing minuscule inclusions of mainly K-feldspar, chlorite and occasionally ilmenite or zircon. K-Feldspars are by no means rare, but are noticeably less dominant than in samples 23OS001 and 23OS003.

4. Discussion

4.1 On the results

4.1.1 Distribution and relationship of radioactive elements

Similarly to the results of previous studies of the RA-granite of Änggårdsbergen, an east-west variation is seemingly present in the Ra-granite of the Säve ridge. However, unlike the increased concentrations of U and Th further to the west in Änggårdsbergen, the relationship in the Säve ridge was found to be more or less the opposite, with generally higher values of both in the eastern parts of the ridge.

This is more obvious in the case of thorium than uranium, as can be seen when one compares Figure 10 to Figure 11. It should be noted that the less clear variations in the uranium concentrations of the Säve ridge (Figure 10) when compared to the thorium concentrations (Figure 11) parallel the results of Elf and Winberg (2019).

Interestingly, unlike previous studies which found no clear spatial relationship in the potassium concentration, the Säve ridge shows a clearly zoned bedrock with higher values in the west and one local hot spot in the east (Figure 9).

The placement of the transect was made with the hypothesis that any variation would be perpendicular to the ridges prevalent in the unit, as had been shown in Änggårdsbergen. Aside from a few local anomalies, this would seem to be the case in the Säve Ridge as well, even after introducing the thin northern row of points.

As mentioned in section 3.3, the only relationship between concentrations of radioactive elements in the Säve RA-granite appears to be the U-Th relationship, as an increase in one of these generally accompanies an increase in the other. As U is potentially mobile under oxidising conditions whereas Th is decidedly not, this seems to rule out a hydrothermal event as the explanation of increasing U concentrations in the central and eastern parts of the ridge. Of note is also that the formula of the U/Th trendline in Säve (Figure 15.C) is very similar to the same formula in Änggårdsbergen (Figure 16), indicating that the enrichment in U and Th likely occurred by the same process in both outcrops and potentially further along the unit.

4.1.2 Magnetic susceptibility

Magnetic susceptibility in rocks depends on the amount of magnetic minerals it contains, which from the samples would mean magnetite and possibly ilmenite in the Säve ridge.

Unlike the central band found in previous studies of Änggårdsbergen, the Säve ridge shows an increased magnetic susceptibility in the eastern part of the ridge. Whilst this coincides with an area of higher potassium content, there is seemingly no direct relationship between these, as illustrated in Figure 15-D.

As the easternmost sample 23OS004 contains relatively plentiful ilmenite, yet shows minimal magnetic susceptibility, it is likely that the magnetic susceptibility is mainly affected by magnetite, of which none is found in the east. As sample 23OS003 contains large grains of FeO but shows a relatively low magnetic susceptibility, these grains are likely hematite and not magnetite. Hematite and magnetite are not possible to distinguish from one another under SEM, and extremely similar under reflected light microscopy. As the grains lack any of the rare distinguishing traits of either

mineral when viewed in polarized light microscopy, magnetic susceptibility presents the only method of distinction.

Given the significantly lower magnetic susceptibility in the east, as well as the much higher degree of alteration, it is likely that any magnetite present in the east has been broken down by hydrothermal alteration and the constituent parts used to form other minerals, such as ilmenite.

Lastly, as magnetic susceptibility is measured with a different instrument to the other parameters, it would seem that point 002, which shows values other than those expected in every variable measured, does not represent an error in instrument operation but rather a true anomaly.

4.1.3 Chemical and mineralogical analysis

A clear difference can be seen between sample 23OS001, located furthest to the west, and 23OS004, located furthest to the east. Sample 23OS001 shows biotite not yet undergoing chloritisation, a generally less fractured texture and K-feldspar as the dominant feldspar. In contrast, sample 23OS004 shows biotite mostly or fully chloritised, a fractured texture with hydrothermal alteration along said fractures and albite as the dominant feldspar.

Sample 23OS003 can be seen as something of an in-between compared to 23OS001 and 23OS004, but resembles 23OS001 much more than 23OS004. The only differences of note between 23OS001 and 23OS003 is the presence of allanite and ilmenite and greater amount of zircon and well-formed iron oxides in the latter.

This explains the REE similarities between sample 23OS003 and 23OS004. As allanite (found in 23OS003) as well as xenotime and monazite (found in 23OS004) host a great deal of REE, as well as radioactive elements uranium and thorium, the presence of these minerals in the central and eastern samples also corresponds to an increase in U and Th concentrations seen in those parts of the ridge.

Allanite and zircon would thus seem to be the main host minerals for the thorium and uranium found in the central parts of the ridge, while xenotime, monazite and zircon act as host minerals in the east. This corresponds well to previous studies from Änggårdsbergen, where uranium and thorium were found in zircon, monazite, allanite (Hultin & Håkansson, 2017) and xenotime (Cooper Svensson & Lundin Frisk, 2018).

From the physical samples, it would seem that the degree of metamorphism and alteration increases to the eastern part of the ridge. Further, as the concentrations of uranium and thorium also increase to the east, it is possible that alteration has been sped up by increased weathering caused by the radioactive elements present there. The only grusified sections found along the width of the ridge were in the middle section, rather than the east, but this might be a consequence of mechanical weathering as a footpath ran across the granite at the site in question. No such footpaths crossed the rock in the east.

Samples from the Säve ridge show a similarly peraluminous composition as samples from Änggårdsbergen (see Figure 21) and also contain a proportionally low Eu concentration in comparison to the rest of the REE (see Figure 20). The low Eu indicates high fractionation and is due to the ability of Eu^{2+} to substitute for Ca^{2+} in Ca-plagioclase (Allaby, 2020), thereby depleting Eu in melts as plagioclase crystallizes or preventing it from joining melt in case of fractional melting should Ca-plagioclase not be molten.

Given the overall similarities in REE, the main chemical difference between RA granite samples is the concentration of Ca and Mg in the samples, which varies considerably (see section 3.5, Figure 23). Other major elements are comparatively similar in concentration between samples.

4.2 On the methods

4.2.1 Sources of error

Though all sites measured by gamma spectrometry were of very good or excellent geometry, dry moss and lichen in vegetation-rich sites might have produced some minor errors in the resulting concentrations. On days when the vegetation was not fully dry, these types of sites were avoided or cleared, but some small amounts of moisture might still have lingered in the weathered and fractured outer edges of the rock. It is unlikely that any errors caused by this would be significant, but it is nevertheless a factor.

Also of note, though the area covered by this study extends nearly 0,9 kilometres across the width of the ridge, it does not cover more than roughly one eighth of the ridge as a whole. Thus, a comparatively small anomaly may have significant impact on the values and the subsequent interpolation.

Finally, and on a similar note to the above, the three physical samples collected from the ridge represent two extremes (23OS001 and 23OS004) and one sample which is not a perfect midpoint (23OS003). Moreover, the samples were not taken at the outermost parts of the ridge, nor did the gamma spectrometry points extend that far, as the edges comprised areas of rough terrain with fewer and less geometrically advantageous rock outcrops. Large boulders also covered the landscape in many places along the edges, which would lead to doubt whether a sample from a rock outcrop would represent the rock of the ridge or the rock of a massive boulder, which might have been deposited there by ice sheets rather than originating in the local rock.

4.2.2 Possible improvements

A larger field area would provide increased certainty of the spatial relationships observed in this study. Similarly, more physical samples from each part of the ridge would allow better pinpointing regarding the chemical changes across the area. It is possible that rather than a gradual change, as is easily theorised from three samples, the smaller ridges constitute distinct subunits with little or no intermingling.

Point 002, which shows unusual values in all variables measured (Figures 9 – 11, 14), has an undue influence upon the interpolated values in that area. As the area is rocky enough to support much denser sampling in the northern part of the study area, such sampling would be likely to either lessen the influence of point 002 or uncover a potentially larger anomaly of which 002 is representative. As such dense sampling far from the initial transect was outside the scope of this study, it was not examined further, but collecting more points and extending the profile further west to the very edge of the ridge might see interesting results.

4.3 Future research

As high-quality data now exists both in Änggårdsbergen and further north in part of the Säve ridge, the natural next step would be to either expand the study area in the Säve ridge or select another rock outcrop of RA-granite in the area between the Säve ridge and Änggårdsbergen. With data from

other sites in the unit, it may be possible to trace stretches of high potassium, uranium or thorium content, as well as magnetic susceptibility, between areas of known values.

It should be noted that the rocks of the Säve ridge form several smaller sub-ridges and valleys running north to south. Following a single such sub-ridge would not be impossible over several kilometres, and may provide refutation or confirmation to the thus far supported hypothesis that the variations within sub-ridges are smaller than the ones between different sub-ridges.

5. Conclusions

- The RA-granite of the Säve ridge is not significantly different from the RA-granite of Änggårdsbergen in chemical composition of either major elements or REE.
- The degree of hydrothermal alteration of the RA-granite of the Säve Ridge increases to the east and lessens to the west.
- There are spatial relationships in the concentration of the radioactive elements in the RA-granite of the Säve ridge.
    - Potassium (K) is greatest in the west.
    - Uranium (U) is greatest in the middle and east.
    - Thorium (Th) is greatest in the east.
- Likewise, there is a spatial relationship in the magnetic susceptibility of the RA-granite of the Säve ridge. The magnetic susceptibility is greatest in the west and decreases to the west.
    - Despite the shared areas of high values, there is no correlation between magnetic susceptibility and Potassium (K) concentration, nor any other radioactive element concentration.
- Uranium (U) is housed in accessory Zircon and likely Allanite. Thorium (Th) is housed mainly in the accessory minerals Allanite, Monazite and Xenotime. Potassium (K) is assumed to reside mainly in potassium feldspars, which are fewer in samples from areas of low K concentration.

6. References

Allaby, M. (2020). Europium anomaly. In *A Dictionary of Geology and Earth Sciences* (5 ed.): Oxford University Press.

Best, M. G. (2003). *Igneous and metamorphic petrology* (2. ed.). Malden : Blackwell Publishers.

Cooper Svensson, J., & Lundin Frisk, E. (2018). Geofysisk och geokemisk kartering av kalium-, uran- och toriumkoncentrationer i Kärragranit inom Änggårdsbergen, Göteborg. In. Gothenburg: Department of Earth Science, University of Gothenburg.

Elf, F., & Winberg, J. (2019). Potassium-, Uranium- and Thorium-concentrations in bedrock. A study of the Sahlgrenska Anomaly and Änggårdsbergen, Gothenburg. In *B-1072*. Gothenburg: Department of Earth Science, University of Gothenburg.

Finck, R. R. (1992). *High resolution field gamma spectrometry and its application to problems in environmental radiology*. Department of Radiation Physics, Malmö and Lund Univ.

Hegardt, E. A., Cornell, D. H., Hellstrom, F. A., & Lundqvist, I. (2007). Emplacement ages of the mid-Proterozoic Kungsbacka bimodal suite, SW Sweden. *GFF*, *129*(3), 227-234. https://doi.org/10.1080/11035890701293227

Hultin, N., & Håkansson, A. (2017). Spatial variation of K-, U-, and Th-concentrations in RA-granite at Änggårdsbergen, southern Gothenburg. In *B-989*. Gothenburg: Department of Earth Science, University of Gothenburg.

Johansson, J. (2014). U och Th fördelning i Bohusgraniten på Bohus-Malmön. In *B-842*. Gothenburg: Department of Earth Science, University of Gothenburg.

Kock, P., & Samuelsson, C. (2011). Comparison of airborne and terrestrial gamma spectrometry measurements - evaluation of three areas in southern Sweden. *Journal of Environmental Radioactivity*, *102*(6), 605-613. https://doi.org/https://doi.org/10.1016/j.jenvrad.2011.03.010

McDonough, W. F., & Sun, S. S. (1995). The composition of the Earth. *Chemical geology*, *120*(3-4), 223-253. https://doi.org/10.1016/0009-2541(94)00140-4

Robb, L. J. (2021). *Introduction to ore-forming processes* (Second edition. ed.). Hoboken, NJ; Chichester, UK : Wiley Blackwell.

Rosenblum, S., & Brownfield, I. K. (1999). *Magnetic Susceptibilities of Minerals*.

Rudnick, R. L., & Fountain, D. M. (1994). Nature and composition of the continental crust. *Eos (Washington, D.C.)*, *75*(44), 72.

Samuelsson, L. (1985). Beskrivning till Berggrundskartan Göteborg NO. In. Uppsala: Sveriges Geologiska Undersökning (SGU).

Tauxe, L., Banerjee, S. K., Butler, R. F., & van der Voo, R. (2018). *Essentials of Paleomagnetism: Fifth Web Edition*

Tennby, G. (2016). Uran- och Toriumfördelning i Stigfjordsgraniten. En kartläggning av uran och toriumhalter i Stigfjordsgraniten på Rönnäng, Tjörn. In *B-953*. Gothenburg: Department of Earth Science, University of Gothenburg.

Wallbrink, P., Walling, D., & He, Q. (2003). Radionuclide measurement using HPGe gamma spectrometry. *Handbook for the assessment of soil erosion and sedimentation using environmental radionuclides*, 67-96.

Appendix I: Figures

A. Sample 23OS004 as thin section under plane polarised light.

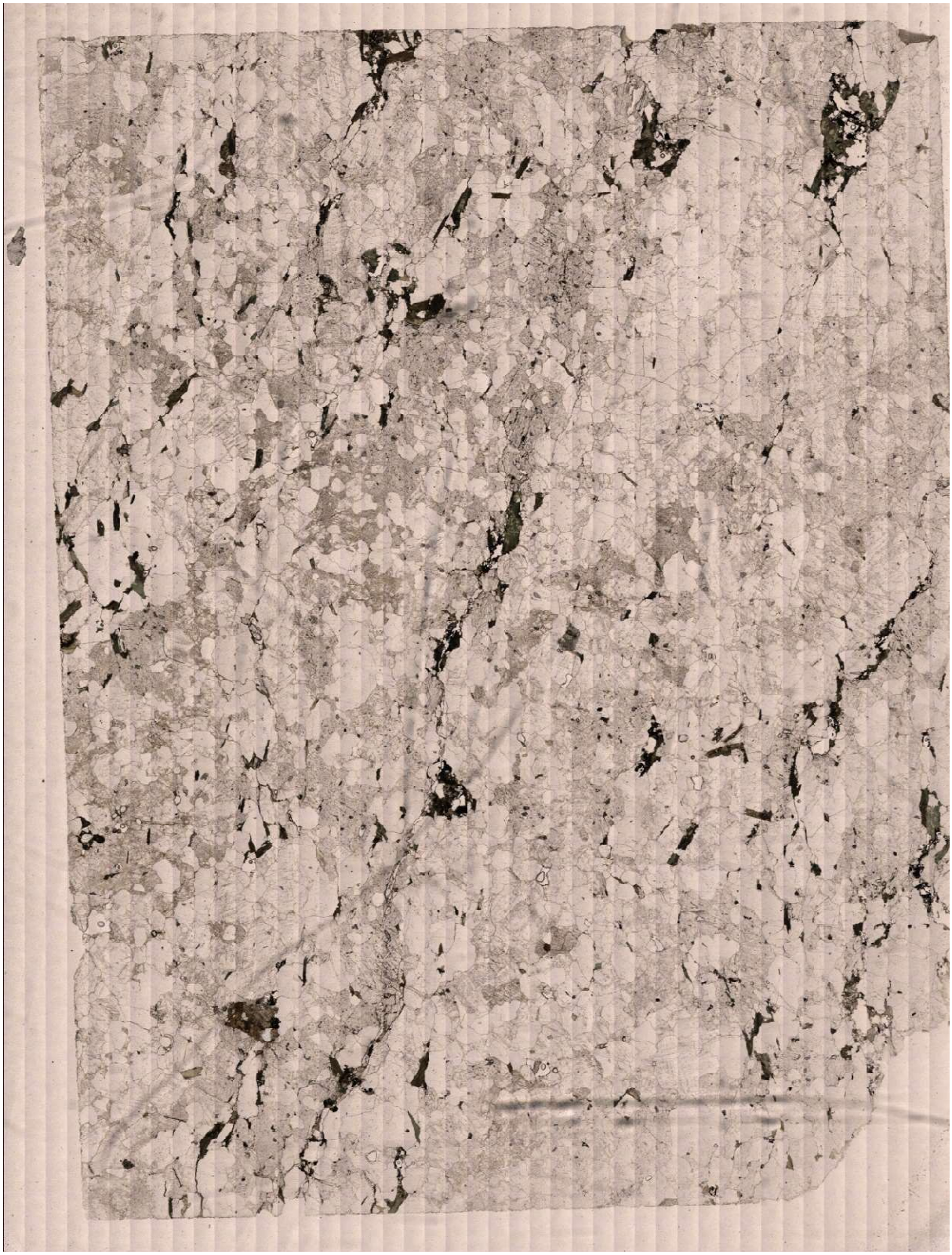

B. Sample 23OS004 as thin section under cross polarised light.

Appendix II: Data

A. Gamma spectrometry and magnetic susceptibility mean values of points taken from the Säve ridge. Point 23OS001 was not suitable for gamma spectrometry but provided a good site for a physical sample, hence the lack of gamma spectrometry values.

Point ID	Lat.	Lon.	K (%)	U (ppm)	Th (ppm)	U/Th	mag. Susc.
23OS001	57,83069	11,93114	-	-	-	-	2092,3
23OS002	57,83122	11,93184	4,73	12,63	47,33	0,267	870,1
23OS003	57,83004	11,93710	4,73	15,60	40,77	0,383	1785,6
23OS004	57,82964	11,94408	3,77	13,43	35,40	0,379	507,7
23OS005	57,83023	11,93143	4,87	6,20	18,50	0,335	6281,7
23OS006	57,83023	11,93162	5,43	6,43	19,43	0,331	3607,5
23OS007	57,83036	11,93174	5,05	7,88	22,35	0,352	3995,8
23OS008	57,83012	11,93225	5,17	5,60	19,53	0,287	2409,2
23OS009	57,83013	11,92246	5,47	6,03	19,27	0,313	2792,5
23OS010	57,83001	11,93302	4,77	6,13	25,53	0,240	5967,5
23OS011	57,82965	11,93283	4,43	11,53	34,50	0,334	4204,4
23OS012	57,82961	11,93298	4,97	9,93	38,37	0,259	7430,8
23OS013	57,82963	11,93321	4,97	10,87	41,27	0,263	4130,0
23OS014	57,82962	11,93342	4,80	7,07	22,37	0,316	5031,7
23OS015	57,82970	11,93373	5,05	7,20	17,70	0,407	3314,2
23OS016	53,83010	11,93417	4,93	7,53	17,30	0,435	4266,9
23OS017	57,82988	11,93438	5,07	7,20	19,47	0,370	6102,5
23OS018	57,82973	11,93420	4,97	7,60	23,57	0,322	6960,0
23OS019	57,82949	11,93440	5,03	6,43	13,13	0,490	4100,0
23OS020	57,82978	11,93461	5,17	6,80	14,73	0,462	4396,7
23OS021	57,82994	11,93481	4,83	6,97	16,43	0,424	5252,5
23OS022	57,83016	11,93601	4,30	10,20	34,80	0,293	1156,3
23OS023	57,82965	11,93618	4,40	10,13	38,63	0,262	1595,0
23OS024	57,82967	11,93628	4,40	9,30	38,33	0,243	1282,5
23OS025	57,82958	11,93662	4,50	12,27	38,30	0,320	1906,7
23OS026	57,82985	11,93659	4,30	9,73	37,70	0,258	1615,8
23OS027	57,82965	11,93679	4,43	11,40	37,30	0,306	2080,0
23OS028	57,82969	11,93702	4,37	19,27	42,93	0,449	538,4
23OS029	57,82984	11,93704	4,47	9,07	38,73	0,234	1814,2
23OS030	57,82976	11,93735	4,47	9,20	33,93	0,271	3981,9
23OS031	57,82973	11,93703	4,27	19,90	42,10	0,473	1617,3
23OS032	57,82954	11,93848	4,53	8,97	37,70	0,238	1140,5
23OS033	57,82953	11,93856	4,33	10,27	31,23	0,329	823,1
23OS034	57,82952	11,93818	4,80	10,40	39,83	0,261	1487,5
23OS035	57,82926	11,93875	4,57	8,67	34,43	0,252	1452,2
23OS036	57,82938	11,93929	4,53	9,70	36,73	0,264	886,3
23OS037	57,82940	11,93919	4,47	9,93	36,67	0,271	861,6
23OS038	57,82949	11,93951	4,63	10,03	38,97	0,257	1276,3
23OS039	57,82928	11,93949	5,00	9,27	44,10	0,210	677,8
23OS040	57,82932	11,93997	4,17	10,07	39,77	0,253	532,3

23OS041	57,82949	11,93978	5,13	10,40	43,27	0,240	404,0
23OS042	57,82948	11,94018	4,40	9,20	38,57	0,239	1014,8
23OS043	57,82925	11,94028	4,37	10,30	39,73	0,259	1163,3
23OS044	57,82922	11,95047	4,80	10,10	41,77	0,242	1355,0
23OS045	57,82936	11,94057	4,70	10,73	43,50	0,247	656,9
23OS046	57,82940	11,94071	4,83	10,83	44,27	0,245	1505,2
23OS047	57,82914	11,94062	4,30	10,67	39,00	0,274	2454,2
23OS048	57,82914	11,94076	3,80	11,00	42,53	0,259	138,6
23OS049	57,82932	11,94106	4,67	10,60	43,53	0,243	2594,2
23OS050	57,82935	11,94111	5,03	12,73	45,27	0,281	1660,8
23OS051	57,82925	11,94130	5,27	11,27	47,33	0,238	1577,5
23OS052	57,82940	11,94144	4,53	9,87	40,00	0,247	1335,3
23OS053	57,82949	11,94167	5,03	11,47	44,83	0,256	1612,3
23OS054	57,82932	11,94180	5,90	11,03	52,33	0,211	1686,9
23OS055	57,82944	11,94203	4,80	10,73	45,87	0,234	1058,6
23OS056	57,82913	11,94224	5,90	16,57	55,97	0,296	2523,1
23OS057	57,82938	11,94238	4,57	11,13	44,10	0,252	1519,7
23OS058	57,82929	11,94261	4,60	10,33	42,50	0,243	1346,2
23OS059	57,82926	11,94283	4,77	10,90	46,03	0,237	1706,0
23OS060	57,82931	11,94320	3,90	11,93	41,03	0,291	1227,8
23OS061	57,82925	11,94353	4,23	9,93	42,07	0,236	1726,3
23OS062	57,82936	11,94368	4,77	7,17	42,20	0,170	1735,0
23OS063	57,82944	11,94397	4,23	9,60	42,20	0,227	688,4
23OS064	57,82943	11,94417	4,90	10,77	43,40	0,248	2524,6
23OS065	57,82929	11,94428	4,47	10,57	40,53	0,261	101,5
23OS066	57,83083	11,94365	4,27	9,83	39,83	0,247	3323,3
23OS067	57,83081	11,94179	4,40	10,23	41,57	0,246	1673,3
23OS068	57,83092	11,94063	4,20	9,33	38,83	0,240	550,8
23OS069	57,83112	11,93746	4,50	8,20	44,70	0,183	361,2
23OS070	57,83092	11,93638	4,23	9,97	40,27	0,248	1738,3
23OS071	57,83122	11,93472	5,27	6,67	25,03	0,266	4963,3
23OS072	57,83149	11,93367	4,80	5,77	15,47	0,373	3256,7
23OS073	57,8308	11,93266	5,07	6,17	20,17	0,306	3285,0

B. Comparison of K, Th and U concentrations in points subjected to both gamma spectrometry and chemical analysis. The difference between the methods is likely due to samples not being taken on the exact location of gamma spectrometry, leading to some variation.

	Gamma Spectrometry			Chemical analysis		
Point ID	K (%)	U (ppm)	Th (ppm)	K2O (%)	U (ppm)	Th (ppm)
23OS003	4,73	15,60	40,77	5,63	7,73	35,6
23OS004	3,77	13,43	35,40	5,96	13,75	48,8

C. Raw values of gamma spectrometry, used to calculate mean values for each point. Values have been rounded to two decimals post mean calculation.

Place ID	Lat.	Lon.	K (%)	U (ppm)	Th (ppm)
a	-	-	-	-	-
b	-	-	-	-	-
c	-	-	-	-	-
23OS001	57,83069	11,93114	-	-	-
a	-	-	4,80	14,00	47,40
b	-	-	4,80	12,20	48,10
c	-	-	4,60	11,70	46,50
23OS002	57,83122	11,93184	4,73	12,63	47,33
a	-	-	5,10	27,80	49,10
b	-	-	4,40	9,50	34,90
c	-	-	4,70	9,50	38,30
23OS003	57,83004	11,9371	4,73	15,60	40,77
a	-	-	4,40	16,50	36,50
b	-	-	4,20	11,00	40,10
c	-	-	2,70	12,80	29,60
23OS004	57,82964	11,94408	3,77	13,43	35,40
a	-	-	4,80	6,50	20,20
b	-	-	4,70	5,90	16,50
c	-	-	5,10	6,20	18,80
23OS005	57,83023	11,93143	4,87	6,20	18,50
a	-	-	5,30	6,50	20,20
b	-	-	5,40	5,70	17,20
c	-	-	5,60	7,10	20,90
23OS006	57,83023	11,93162	5,43	6,43	19,43
a	-	-	4,90	8,10	22,90
b	-	-	5,20	9,00	24,20
c	-	-	4,90	6,50	20,90
d	-	-	5,20	7,90	21,40
23OS007	57,83036	11,93174	5,05	7,88	22,35
a	-	-	5,20	5,80	19,60
b	-	-	5,20	5,00	19,90
c	-	-	5,10	6,00	19,10
23OS008	57,83012	11,93225	5,17	5,60	19,53
a	-	-	5,60	6,70	19,40
b	-	-	5,20	5,90	19,80
c	-	-	5,60	5,50	18,60
23OS009	57,83013	11,92246	5,47	6,03	19,27
a	-	-	4,70	5,80	25,50
b	-	-	4,90	4,60	24,00
c	-	-	4,70	8,00	27,10
23OS010	57,83001	11,93302	4,77	6,13	25,53
a	-	-	4,60	15,30	29,80
b	-	-	4,30	11,30	35,70
c	-	-	4,30	8,10	37,50
d	-	-	4,50	11,40	35,00

23OS011	57,82965	11,93283	4,43	11,53	34,50
a	-	-	5,10	10,60	38,60
b	-	-	4,80	9,10	34,90
c	-	-	5,00	10,10	41,60
23OS012	57,82961	11,93298	4,97	9,93	38,37
a	-	-	4,90	11,30	41,30
b	-	-	4,70	10,30	37,80
c	-	-	5,30	11,00	44,70
23OS013	57,82963	11,93321	4,97	10,87	41,27
a	-	-	5,00	7,60	22,30
b	-	-	4,70	6,70	26,70
c	-	-	4,70	6,90	18,10
23OS014	57,82962	11,93342	4,80	7,07	22,37
a	-	-	5,20	6,00	16,40
b	-	-	5,10	6,30	17,90
c	-	-	5,00	9,30	20,20
d	-	-	4,90	7,20	16,30
23OS015	57,8297	11,93373	5,05	7,20	17,70
a	-	-	5,10	7,20	17,40
b	-	-	5,00	6,40	15,00
c	-	-	4,70	9,00	19,50
23OS016	53,8301	11,93417	4,93	7,53	17,30
a	-	-	5,10	6,80	19,30
b	-	-	5,10	6,60	19,20
c	-	-	5,00	8,20	19,90
23OS017	57,82988	11,93438	5,07	7,20	19,47
a	-	-	5,30	7,80	30,30
b	-	-	4,80	7,90	21,00
c	-	-	4,80	7,10	19,40
23OS018	57,82973	11,9342	4,97	7,60	23,57
a	-	-	4,90	5,20	12,10
b	-	-	5,00	7,70	13,60
c	-	-	5,20	6,40	13,70
23OS019	57,82949	11,9344	5,03	6,43	13,13
a	-	-	5,20	6,50	13,50
b	-	-	5,20	7,10	15,10
c	-	-	5,10	6,80	15,60
23OS020	57,82978	11,93461	5,17	6,80	14,73
a	-	-	5,10	6,80	14,90
b	-	-	4,90	7,40	16,40
c	-	-	4,50	6,70	18,00
23OS021	57,82994	11,93481	4,83	6,97	16,43
a	-	-	4,30	11,50	36,10
b	-	-	4,30	9,10	31,90
c	-	-	4,30	10,00	36,40
23OS022	57,83016	11,93601	4,30	10,20	34,80
a	-	-	4,30	10,30	39,60
b	-	-	4,50	10,60	36,60
c	-	-	4,40	9,50	39,70

23OS023	57,82965	11,93618	4,40	10,13	38,63
a	-	-	4,40	8,30	39,10
b	-	-	4,30	9,70	37,00
c	-	-	4,50	9,90	38,90
23OS024	57,82967	11,93628	4,40	9,30	38,33
a	-	-	4,60	10,90	37,20
b	-	-	4,20	13,20	39,30
c	-	-	4,70	12,70	38,40
23OS025	57,82958	11,93662	4,50	12,27	38,30
a	-	-	4,30	9,80	36,30
b	-	-	4,40	9,70	36,20
c	-	-	4,20	9,70	40,60
23OS026	57,82985	11,93659	4,30	9,73	37,70
a	-	-	4,60	10,60	37,30
b	-	-	4,40	11,20	37,70
c	-	-	4,30	12,40	36,90
23OS027	57,82965	11,93679	4,43	11,40	37,30
a	-	-	4,30	19,70	41,90
b	-	-	4,70	16,30	43,90
c	-	-	4,10	21,80	43,00
23OS028	57,82969	11,93702	4,37	19,27	42,93
a	-	-	4,20	8,30	39,10
b	-	-	4,50	9,80	37,50
c	-	-	4,70	9,10	39,60
23OS029	57,82984	11,93704	4,47	9,07	38,73
a	-	-	4,50	8,90	33,90
b	-	-	4,90	8,60	37,20
c	-	-	4,00	10,10	30,70
23OS030	57,82976	11,93735	4,47	9,20	33,93
a	-	-	4,30	20,80	41,40
b	-	-	4,20	20,30	42,30
c	-	-	4,30	18,60	42,60
23OS031	57,82973	11,93703	4,27	19,90	42,10
a	-	-	4,50	9,50	36,70
b	-	-	4,60	8,60	37,50
c	-	-	4,50	8,80	38,90
23OS032	57,82954	11,93848	4,53	8,97	37,70
a	-	-	4,30	10,00	31,70
b	-	-	4,20	11,70	27,60
c	-	-	4,50	9,10	34,40
23OS033	57,82953	11,93856	4,33	10,27	31,23
a	-	-	5,00	9,20	42,70
b	-	-	4,50	10,50	36,00
c	-	-	4,90	11,50	40,80
23OS034	57,82952	11,93818	4,80	10,40	39,83
a	-	-	4,60	8,00	35,60
b	-	-	4,50	9,30	35,60
c	-	-	4,60	8,70	32,10
23OS035	57,82926	11,93875	4,57	8,67	34,43

a	-	-	4,70	10,60	38,30
b	-	-	4,40	10,20	34,70
c	-	-	4,50	8,30	37,20
23OS036	57,82938	11,93929	4,53	9,70	36,73
a	-	-	4,40	9,60	36,10
b	-	-	4,70	9,70	36,40
c	-	-	4,30	10,50	37,50
23OS037	57,8294	11,93919	4,47	9,93	36,67
a	-	-	4,70	8,90	38,30
b	-	-	4,60	11,10	36,90
c	-	-	4,60	10,10	41,70
23OS038	57,82949	11,93951	4,63	10,03	38,97
a	-	-	4,90	9,00	44,40
b	-	-	5,10	9,50	46,00
c	-	-	5,00	9,30	41,90
23OS039	57,82928	11,93949	5,00	9,27	44,10
a	-	-	4,30	9,50	40,10
b	-	-	4,00	10,40	38,10
c	-	-	4,20	10,30	41,10
23OS040	57,82932	11,93997	4,17	10,07	39,77
a	-	-	5,00	11,00	44,00
b	-	-	5,10	10,30	44,50
c	-	-	5,30	9,90	41,30
23OS041	57,82949	11,93978	5,13	10,40	43,27
a	-	-	4,50	10,10	37,90
b	-	-	4,40	8,60	37,30
c	-	-	4,30	8,90	40,50
23OS042	57,82948	11,94018	4,40	9,20	38,57
a	-	-	4,60	9,60	39,20
b	-	-	4,20	10,70	39,40
c	-	-	4,30	10,60	40,60
23OS043	57,82925	11,94028	4,37	10,30	39,73
a	-	-	4,80	10,10	40,80
b	-	-	4,70	9,80	43,40
c	-	-	4,90	10,40	41,10
23OS044	57,82922	11,95047	4,80	10,10	41,77
a	-	-	4,70	10,60	43,20
b	-	-	4,60	11,60	42,70
c	-	-	4,80	10,00	44,60
23OS045	57,82936	11,94057	4,70	10,73	43,50
a	-	-	4,70	10,50	43,60
b	-	-	4,90	10,90	43,40
c	-	-	4,90	11,10	45,80
23OS046	57,8294	11,94071	4,83	10,83	44,27
a	-	-	4,30	10,70	36,70
b	-	-	4,20	10,30	39,90
c	-	-	4,40	11,00	40,40
23OS047	57,82914	11,94062	4,30	10,67	39,00
a	-	-	4,00	10,20	44,60

b	-	-	3,70	12,50	40,40
c	-	-	3,70	10,30	42,60
23OS048	57,82914	11,94076	3,80	11,00	42,53
a	-	-	4,70	10,00	42,80
b	-	-	4,60	11,20	44,00
c	-	-	4,70	10,60	43,80
23OS049	57,82932	11,94106	4,67	10,60	43,53
a	-	-	5,20	13,50	46,80
b	-	-	5,00	11,50	44,70
c	-	-	4,90	13,20	44,30
23OS050	57,82935	11,94111	5,03	12,73	45,27
a	-	-	5,30	12,00	44,90
b	-	-	5,20	10,60	48,70
c	-	-	5,30	11,20	48,40
23OS051	57,82925	11,9413	5,27	11,27	47,33
a	-	-	4,50	11,30	40,10
b	-	-	4,50	8,40	39,80
c	-	-	4,60	9,90	40,10
23OS052	57,8294	11,94144	4,53	9,87	40,00
a	-	-	4,90	10,90	46,70
b	-	-	5,20	11,10	44,40
c	-	-	5,00	12,40	43,40
23OS053	57,82949	11,94167	5,03	11,47	44,83
a	-	-	5,90	11,80	52,90
b	-	-	5,90	10,40	51,30
c	-	-	5,90	10,90	52,80
23OS054	57,82932	11,9418	5,90	11,03	52,33
a	-	-	4,70	10,90	45,40
b	-	-	4,80	11,10	47,60
c	-	-	4,90	10,20	44,60
23OS055	57,82944	11,94203	4,80	10,73	45,87
a	-	-	6,20	17,00	58,10
b	-	-	5,50	16,50	53,00
c	-	-	6,00	16,20	56,80
23OS056	57,82913	11,94224	5,90	16,57	55,97
a	-	-	4,40	11,20	42,40
b	-	-	4,60	11,90	45,40
c	-	-	4,70	10,30	44,50
23OS057	57,82938	11,94238	4,57	11,13	44,10
a	-	-	4,60	10,00	42,50
b	-	-	4,70	10,40	40,70
c	-	-	4,50	10,60	44,30
23OS058	57,82929	11,94261	4,60	10,33	42,50
a	-	-	4,70	11,00	47,20
b	-	-	4,80	10,70	43,70
c	-	-	4,80	11,00	47,20
23OS059	57,82926	11,94283	4,77	10,90	46,03
a	-	-	4,00	12,70	42,70
b	-	-	3,90	11,20	39,60

c	-	-	3,80	11,90	40,80
23OS060	57,82931	11,9432	3,90	11,93	41,03
a	-	-	4,20	9,80	40,40
b	-	-	4,20	9,70	45,00
c	-	-	4,30	10,30	40,80
23OS061	57,82925	11,94353	4,23	9,93	42,07
a	-	-	4,70	7,60	43,40
b	-	-	5,00	5,90	37,00
c	-	-	4,60	8,00	46,20
23OS062	57,82936	11,94368	4,77	7,17	42,20
a	-	-	4,30	9,70	43,20
b	-	-	4,00	9,10	40,50
c	-	-	4,40	10,00	42,90
23OS063	57,82944	11,94397	4,23	9,60	42,20
a	-	-	4,70	10,90	43,30
b	-	-	4,90	11,10	41,90
c	-	-	5,10	10,30	45,00
23OS064	57,82943	11,94417	4,90	10,77	43,40
a	-	-	4,60	10,70	40,40
b	-	-	4,40	10,20	39,90
c	-	-	4,40	10,80	41,30
23OS065	57,82929	11,94428	4,47	10,57	40,53
a	-	-	4,30	9,90	42,60
b	-	-	4,30	9,70	37,60
c	-	-	4,20	9,90	39,30
23OS066	57,83083	11,94365	4,27	9,83	39,83
a	-	-	4,60	10,50	40,70
b	-	-	4,30	9,70	41,90
c	-	-	4,30	10,50	42,10
23OS067	57,83081	11,94179	4,40	10,23	41,57
a	-	-	4,30	9,00	40,10
b	-	-	4,10	9,50	37,40
c	-	-	4,20	9,50	39,00
23OS068	57,83092	11,94063	4,20	9,33	38,83
a	-	-	4,00	6,80	41,30
b	-	-	4,50	6,90	40,30
c	-	-	5,00	10,90	52,50
23OS069	57,83112	11,93746	4,50	8,20	44,70
a	-	-	4,20	10,10	42,70
b	-	-	4,20	9,70	37,90
c	-	-	4,30	10,10	40,20
23OS070	57,83092	11,93638	4,23	9,97	40,27
a	-	-	5,30	7,30	28,80
b	-	-	5,40	6,00	21,10
c	-	-	5,10	6,70	25,20
23OS071	57,83122	11,93472	5,27	6,67	25,03
a	-	-	4,80	5,70	15,90
b	-	-	4,70	5,80	15,20
c	-	-	4,90	5,80	15,30

23OS072	57,83149	11,93367	4,80	5,77	15,47
a	-	-	5,10	5,80	20,60
b	-	-	5,10	7,00	19,30
c	-	-	5,00	5,70	20,60
23OS073	57,8308	11,93266	5,07	6,17	20,17

D. Magnetic susceptibility measurements of the Säve ridge. Minimum, maximum and median rounded to nearest whole number, mean rounded to nearest decimal.

Point ID	Lat.	Lon.	# of surveys	Min	Max	Median	Mean
23OS001	57,83069	11,93114	12	753	3960	1895	2092,3
23OS002	57,83122	11,93184	16	40	3860	311	870,1
23OS003	57,83004	11,93710	12	767	3860	1720	1785,6
23OS004	57,82964	11,94408	12	53	1520	109	507,7
23OS005	57,83023	11,93143	12	4140	7720	6445	6281,7
23OS006	57,83023	11,93162	12	2980	4470	3445	3607,5
23OS007	57,83036	11,93174	12	3230	5390	3940	3995,8
23OS008	57,83012	11,93225	12	2030	2900	2370	2409,2
23OS009	57,83013	11,92246	12	1900	3850	2835	2792,5
23OS010	57,83001	11,93302	12	3650	6990	6355	5967,5
23OS011	57,82965	11,93283	9	2810	5520	4350	4204,4
23OS012	57,82961	11,93298	12	5260	9780	7810	7430,8
23OS013	57,82963	11,93321	12	2690	5640	4120	4130,0
23OS014	57,82962	11,93342	12	4100	7200	4925	5031,7
23OS015	57,82970	11,93373	12	2410	3870	3395	3314,2
23OS016	53,83010	11,93417	16	2720	7240	3940	4266,9
23OS017	57,82988	11,93438	16	4710	7420	5925	6102,5
23OS018	57,82973	11,93420	16	3350	9800	6775	6960,0
23OS019	57,82949	11,93440	12	2900	5540	3925	4100,0
23OS020	57,82978	11,93461	12	2250	6780	4295	4396,7
23OS021	57,82994	11,93481	12	4210	6440	5325	5252,5
23OS022	57,83016	11,93601	12	404	1550	1220	1156,3
23OS023	57,82965	11,93618	12	1300	1910	1595	1595,0
23OS024	57,82967	11,93628	12	1040	1620	1260	1282,5
23OS025	57,82958	11,93662	12	1510	2350	1895	1906,7
23OS026	57,82985	11,93659	12	1190	1960	1675	1615,8
23OS027	57,82965	11,93679	12	1360	3270	2130	2080,0
23OS028	57,82969	11,93702	12	159	1780	456	538,4
23OS029	57,82984	11,93704	12	1240	2400	1790	1814,2
23OS030	57,82976	11,93735	16	287	8200	3610	3981,9
23OS031	57,82973	11,93703	16	129	4900	613	1617,3
23OS032	57,82954	11,93848	12	936	1610	1110	1140,5
23OS033	57,82953	11,93856	12	616	1100	786	823,1
23OS034	57,82952	11,93818	12	1210	1710	1530	1487,5
23OS035	57,82926	11,93875	12	854	2430	1430	1452,2
23OS036	57,82938	11,93929	12	295	1290	927	886,3
23OS037	57,82940	11,93919	12	537	1130	898	861,6
23OS038	57,82949	11,93951	12	566	1660	1390	1276,3
23OS039	57,82928	11,93949	12	482	954	688	677,8

23OS040	57,82932	11,93997	12	415	674	510	532,3
23OS041	57,82949	11,93978	12	119	536	414	404,0
23OS042	57,82948	11,94018	12	572	1310	1035	1014,8
23OS043	57,82925	11,94028	12	665	1630	1240	1163,3
23OS044	57,82922	11,95047	12	1040	1720	1360	1355,0
23OS045	57,82936	11,94057	12	413	886	646	656,9
23OS046	57,82940	11,94071	12	772	2280	1500	1505,2
23OS047	57,82914	11,94062	12	1570	2780	2585	2454,2
23OS048	57,82914	11,94076	12	12	187	149	138,6
23OS049	57,82932	11,94106	12	1720	4210	2425	2594,2
23OS050	57,82935	11,94111	12	579	2640	1655	1660,8
23OS051	57,82925	11,94130	12	1230	2210	1550	1577,5
23OS052	57,82940	11,94144	12	854	1790	1340	1335,3
23OS053	57,82949	11,94167	12	278	2390	1695	1612,3
23OS054	57,82932	11,94180	12	463	2310	1800	1686,9
23OS055	57,82944	11,94203	12	456	1770	1024	1058,6
23OS056	57,82913	11,94224	16	1010	3640	2660	2523,1
23OS057	57,82938	11,94238	12	623	2190	1585	1519,7
23OS058	57,82929	11,94261	12	780	1930	1335	1346,2
23OS059	57,82926	11,94283	12	992	2310	1705	1706,0
23OS060	57,82931	11,94320	12	698	2230	1165	1227,8
23OS061	57,82925	11,94353	12	916	2250	1760	1726,3
23OS062	57,82936	11,94368	16	169	4590	1355	1735,0
23OS063	57,82944	11,94397	16	86	2340	388	688,4
23OS064	57,82943	11,94417	13	1560	3790	2410	2524,6
23OS065	57,82929	11,94428	12	66	137	97	101,5
23OS066	57,83083	11,94365	12	1690	4890	3295	3323,3
23OS067	57,83081	11,94179	12	920	2280	1695	1673,3
23OS068	57,83092	11,94063	12	274	816	531	550,8
23OS069	57,83112	11,93746	12	53	2010	106	361,2
23OS070	57,83092	11,93638	12	1230	2270	1775	1738,3
23OS071	57,83122	11,93472	12	4030	6310	4895	4963,3
23OS072	57,83149	11,93367	12	2030	5000	3005	3256,7
23OS073	57,8308	11,93266	12	2500	3830	3320	3285,0

E. Chemistry of RA-granite samples from Änggårdsbergen and the Säve ridge.

SAMPLE	unit	16FF200	17FF02	17FF04	17ANH009	17ANH030	18AJE1	18AJE4	19FJ001	19FJ006	23OS001	23OS003	23OS004
SiO2	%	61,7	74,4	76,1	77	77,3	75,8	79,5	81	65,4	71,9	75,9	74
Al2O3	%	17,15	12,3	10,55	11,65	11,9	12,7	10,65	9	17,5	13,4	12	13,05
Fe2O3	%	5,21	4,04	4,38	1,99	1,52	2,17	1,63	4,22	2,46	2,66	2,67	2,55
CaO	%	0,28	0,5	0,13	0,21	0,43	0,4	0,06	0,31	0,78	0,69	0,6	0,12
MgO	%	0,6	0,02	0,03	0,24	0,22	0,28	0,24	0,22	1,29	0,47	0,03	0,13
Na2O	%	1,58	3,69	4,04	3,78	2,63	3,95	2,63	2,27	5,33	2,8	3,19	3,43
K2O	%	11,95	5,03	4,95	4,38	5,48	4,42	4,87	3,82	5,91	6,49	5,63	5,96
Cr2O3	%	<0.01	<0.01	<0.01	<0.01	<0.01	0,024	0,013	0,004	0,004	<0.002	<0.002	<0.002
TiO2	%	0,49	0,36	0,3	0,23	0,22	0,22	0,22	0,21	0,38	0,48	0,21	0,38
Th	ppm	201	42,2	79,6	56,6	60,6	41	77,3	49,9	55,4	29,1	35,6	48,8
U	ppm	19,35	10,15	14,85	9,17	19,7	12,4	7,61	14,05	10,9	8,27	7,73	13,75
La	ppm	1708,86	715,19	419,83	315,19	39,24	378,06	37,55	372,15	308,44	163,71	556,96	540,08
Ce	ppm	1450,24	670,47	391,52	293,64	38,99	265,09	58,89	357,26	221,86	224,31	474,71	481,24
Pr	ppm	983,84	459,05	238,15	181,03	26,40	227,37	27,48	244,61	166,49	108,84	371,77	365,30
Nd	ppm	713,35	354,49	175,93	132,60	18,60	169,37	19,04	177,24	104,16	73,52	264,77	252,74
Sm	ppm	430,41	230,41	107,77	75,00	17,16	97,97	16,55	118,92	55,88	44,53	162,16	145,95
Eu	ppm	56,66	30,73	12,61	7,82	2,49	12,61	2,13	12,61	12,79	9,59	23,62	26,64
Gd	ppm	295,98	151,76	75,13	38,29	15,38	60,55	17,29	83,92	37,09	30,60	112,06	99,50
Tb	ppm	259,28	145,71	79,50	39,34	23,27	55,68	21,61	91,97	32,69	31,02	97,23	89,20
Dy	ppm	228,46	132,11	81,30	38,01	26,71	51,83	24,51	91,46	29,23	30,12	87,40	82,93
Ho	ppm	189,56	110,62	75,46	38,28	29,30	45,79	28,02	99,27	27,84	29,85	84,07	82,42
Er	ppm	190,00	109,69	84,38	42,06	34,13	48,38	33,13	106,56	28,88	31,13	81,88	80,63
Tm	ppm	180,57	107,69	92,31	48,18	40,89	51,01	36,03	116,60	29,55	31,98	83,40	80,97
Yb	ppm	168,94	104,04	98,14	52,48	45,53	53,48	43,48	115,22	31,74	34,72	84,78	82,30
Lu	ppm	156,91	99,59	99,59	53,25	46,34	46,34	36,99	104,47	29,27	32,93	82,93	82,93